

MASSACHUSETTS INSTITUTE OF TECHNOLOGY  
LINCOLN LABORATORY

*ADA 277459*

**AN ADAPTIVE RADIO-FREQUENCY HYPERTHERMIA  
PHASED-ARRAY SYSTEM FOR IMPROVED CANCER  
THERAPY: PHANTOM TARGET MEASUREMENTS**

*A.J. FENN  
Group 63*

*G.A. KING*

*State University of New York Health Science Center*

TECHNICAL REPORT 999

19-NOVEMBER 1993

Accession For	
NTIS CRA&I	<input checked="" type="checkbox"/>
DTIC TAB	<input type="checkbox"/>
Unannounced	<input type="checkbox"/>
Justification	
By	
Distribution/	
Availability Codes	
Dist	Avail and/or Special
A-1	

Approved for public release; distribution is unlimited.

This report is based on studies performed at Lincoln Laboratory, a center for research operated by Massachusetts Institute of Technology. The work was sponsored by the Department of the Air Force and the MIT Technology Licensing Office under Air Force Contract F19628-90-C-0002.

This report may be reproduced to satisfy needs of U.S. Government agencies.

The ESC Public Affairs Office has reviewed this report, and it is releasable to the National Technical Information Service, where it will be available to the general public, including foreign nationals.

This technical report has been reviewed and is approved for publication.

FOR THE COMMANDER

  
Gary Tutungian  
Administrative Contracting Officer  
Directorate of Contracted Support Management

Non-Lincoln Recipients

PLEASE DO NOT RETURN

Permission is given to destroy this document  
when it is no longer needed.

BEST AVAILABLE COPY

## ABSTRACT

An adaptive radio-frequency hyperthermia system for improved therapeutic tumor heating is investigated. Adaptive array techniques are used to modify the electric-field and temperature distribution in hyperthermia experiments with phantom targets. A commercial hyperthermia phased-array antenna system at the SUNY Health Science Center in Syracuse, New York, has been modified to implement adaptive nulling and adaptive focusing algorithms. The hyperthermia system is the BSD Medical Corporation Model BSD-2000 with Sigma-60 annular phased-array antenna applicator. The applicator operates from 60 to 120 MHz and consists of four pairs of dipole antenna radiators. The four-channel transmit array is made adaptive by software modifications which invoke a gradient-search feedback algorithm. The gradient-search algorithm implements the method of steepest descent for adaptive nulling and the method of steepest ascent for adaptive focusing. The feedback signals are provided by electric-field short-dipole probe antennas.

With the proposed adaptive hyperthermia array design concept, it may be possible to maximize the applied electric field at a tumor position in the target body and simultaneously minimize or reduce the electric field at target positions where undesired high-temperature regions (hot spots) occur. The measured phantom-target data indicate that adaptive nulling can reduce the electric field at one or more target positions while simultaneously focusing at a deep-seated position within the target.

## ACKNOWLEDGMENTS

The support of the Lincoln Laboratory Advanced Concepts Committee is sincerely appreciated. Technical discussions with Paul F. Turner of BSD Medical Corporation are also appreciated. The software support of Jan Robbins, also of BSD Medical Corporation, has been very helpful in this study. Dr. Fenn wishes to express his gratitude to D.H. Temme of MIT Lincoln Laboratory for technical discussions and to J.F. Fitzgerald and L.S. Dipalma for technical assistance.

## TABLE OF CONTENTS

Abstract	iii
Acknowledgments	v
List of Illustrations	ix
1. INTRODUCTION	1
2. THEORY	9
2.1 Noninvasive Adaptive Hyperthermia System Concept	9
2.2 Adaptive Transmit-Array Formulation	11
2.3 System Considerations	16
3. MATERIALS AND METHODS	21
4. MEASURED RESULTS	29
4.1 One Adaptive Null for Cylindrical Phantom	29
4.2 Two Adaptive Nulls for Cylindrical Phantom	32
4.3 Adaptive Focus for Cylindrical Phantom	35
4.4 One Adaptive Null for Beef Phantom	35
5. CONCLUSION	41
APPENDIX A - Measured Electric-Field Probe Raw Data	43
REFERENCES	49

## LIST OF ILLUSTRATIONS

Figure No.		Page
1	A clinical hyperthermia phased-array antenna system (photograph courtesy of BSD Medical Corporation).	3
2	(a) Transverse cross section at the prostate level. An eight-element hyperthermia ring array of dipole elements is used to irradiate a target body with sufficient power to elevate the tumor temperature in the target body to a therapeutic level. (b) Elliptical phantom target used to model the prostate (target)-level cross section. Shown are four noninvasive auxiliary E-field probes that are used in forming null zones with widths controlled by the individual null strengths. The null zones extend into the body to reduce the internal electric field at specified locations.	5
3	Simulated two-dimensional thermal pattern in elliptical phantom muscle-tissue target surrounded with 10°C constant-temperature water bolus. The incident RF power distribution is at 120 MHz and the initial temperature of the phantom is 25°C. Temperature contour levels are given in 2°C steps. (a) Before nulling; hot spots on the left and right sides of the target are present. (b) After nulling; hot spots are eliminated.	6
4	Noninvasive adaptive hyperthermia system concept.	10
5	Scatter diagram in rectangular coordinates for the amplitude and phase of the transmit weights in a hyperthermia phased-array antenna. The $n$ th transmit weight in the $j$ th configuration of transmit weights is denoted $w_{nj}$ .	13
6	Figure of merit with transmit-weight dithering for optimum search directions.	17
7	Gradient-search algorithm block diagram for adaptive-nulling hyperthermia system.	18
8	Hyperthermia treatment facility at the Health Science Center, State University of New York.	22
9	BSD-2000 Sigma-60 applicator on patient-support assembly at SUNY.	23
10	BSD-2000 transmitter rack.	24
11	BSD-2000 Sigma-60 applicator with coaxial feedlines.	25
12	Saline-filled cylindrical phantom with dipole probe and temperature/electric-field monitoring unit.	26
13	Front face dimensions and probe positions for beef phantom.	28

## LIST OF ILLUSTRATIONS (Continued)

Figure No.		Page
14	Experimental test setup for the saline-filled cylindrical phantom. Three probes are used to monitor the electric field during the adaptive-nulling measurements.	30
15	Beef phantom target with electric-field probes and thermocouples.	31
16	Experimental demonstration of an adaptive-nulling hyperthermia system at SUNY. The figure shows the measured electric field as a function of adaptive-nulling gradient-search iteration number for a saline-filled cylindrical phantom. One adaptive null is formed at probe position 2.	33
17	Measured electric field as a function of adaptive-nulling gradient-search iteration number for a saline-filled cylindrical phantom. Two adaptive nulls are formed at probe positions 2 and 3. Notice that the power measured by the invasive electric-field probe is relatively constant over the 50 iterations.	34
18	Measured electric field in a longitudinal cut on the surface of the cylindrical phantom before and after nulling.	36
19	Measured electric field as a function of adaptive-phase-focusing gradient-search iteration number for a saline-filled cylindrical phantom. The power level at the focus increases by 0.8 dB due to the adaptive gradient search.	37
20	Measured electric field as a function of adaptive-nulling gradient-search iteration number for a beef phantom. One adaptive null is formed at probe position 2.	39
21	Measured temperatures in the beef phantom. Eighty minutes after the start of the experiment, a 4°C higher temperature exists at the tumor site compared to the null site.	40

## 1. INTRODUCTION

Adaptive array antennas are well known for their ability to improve the performance of communications and radar systems [1, 2]. Recently, adaptive array techniques have been applied to the medical application of radio-frequency (RF) hyperthermia for deep-seated tumor therapy [3-6]. With an adaptive radio-frequency hyperthermia array, it is theoretically possible to automatically control the RF electric field at multiple positions within the target body [3-6]. The electric field radiated by a hyperthermia phased array can be minimized (nulled) and maximized (focused) at desired target positions by adaptively adjusting the transmit amplifiers and phase shifters of the hyperthermia apparatus. In this report, multiple adaptive electric-field nulls and adaptive focusing are experimentally demonstrated at the State University of New York (SUNY) Health Science Center with a modified commercial hyperthermia phased-array system and phantom target measurements [7].

The treatment of deep-seated malignant tumors within a patient is often a difficult task. The objective of the treatment is to reduce in size or completely remove the tumor mass by one or more modalities available at the treatment facility. Common modalities are surgery, chemotherapy, and x-ray therapy [8]. A particular modality used alone or in conjunction with another modality is "tissue heating," or hyperthermia [8-12]. Hyperthermia can be considered as a form of high fever within the body; a controlled thermal dose distribution is required for hyperthermia to have a therapeutic value. Typical localized-hyperthermia temperatures required for therapeutic treatment of cancer are in the 42.5°-45°C range. Normal tissue should be kept at temperatures below 42.5°C during the treatment. The most difficult aspect of implementing hyperthermia, with either radio-frequency waves or acoustic (ultrasound) waves, is producing sufficient heating at depth. Multiple-applicator RF hyperthermia arrays are commonly used to provide a focused main beam at the tumor position. A focal region should be concentrated at the tumor with minimal energy delivered to surrounding normal tissue. As the hyperthermia antenna beamwidth is proportional to the wavelength, a small focal region suggests that the RF wavelength be as small as possible. However, due to propagation losses in tissue, the RF depth of penetration decreases with increasing transmit frequency. One of the major problems in heating a deep-seated tumor with a hyperthermia antenna is the formation of undesired "hot spots" in surrounding tissue. This additional undesired heating often produces pain, burns, and blistering in the patient, which requires terminating the treatment. Thus, techniques for reducing hot spots are necessary in hyperthermia treatment.

A typical clinical RF hyperthermia treatment consists of several two-hour sessions spread over a period of several weeks. During a two-hour session, the first hour is used for patient preparation, during which temperature and vital-signs monitoring instrumentation are interfaced with the patient. After the patient is readied, the hyperthermia antenna RF signal is turned on and the tumor is heated by the radiated electromagnetic energy. The tumor should be heated for approximately 45 minutes at a temperature of 42.5°-45°C. Approximately 15 minutes (maximum) is available prior to the actual delivery of RF energy to the tumor for manually or adaptively shaping the RF electric-field distribution within the patient target tissue. Current clinical operation of

hyperthermia phased arrays allows limited manual control of the array transmit-element gain and phase. Some improvement in the electric-field distribution can be achieved by this manual trial-and-error method, but automatic adjustment techniques, offered by adaptive arrays, are desirable and possibly offer better electric-field distributions.

Several journals have published special issues on acoustic and electromagnetic hyperthermia treatment of cancer [13, 14]. Electromagnetic transmitting arrays in the frequency band 60–2000 MHz are used to localize heating of malignant tumors within a target body. Many studies have been conducted to produce improved therapeutic field distributions with hyperthermia phased arrays [15–32]. Phase control can be used to synthesize improved RF radiation patterns without adaptive control of the transmit-array weights [15–20]. Array transmit weights can be adaptively controlled to maximize the tumor temperature (or RF power delivered to the tumor) while minimizing the surrounding tissue temperature (or RF power delivered to the surrounding tissue) [21–32]. All other studies require invasive techniques to optimize the radiation pattern [21–32]. A previous report [3] and several conference articles [4–6] investigate the theoretical benefit of using adaptive nulling with noninvasive auxiliary dipole sensors to reduce the field intensity at selected positions in the target body while maintaining a desired focus at a tumor. Multiple adaptive electric-field nulls were used to show a theoretical reduction in hot spots for a homogeneous elliptical phantom target surrounded by a water bolus and hyperthermia ring array [3–6].

The hyperthermia annular phased-array antenna system (Model BSD-2000, SIGMA-60 applicator [33], BSD Medical Corporation, Salt Lake City, Utah) used in these experiments is shown in Figure 1. <sup>1</sup> By fully surrounding the patient with an annular phased array, it is possible to obtain constructive interference (or signal enhancement) deep within the target volume. The BSD-2000 hyperthermia system uses a 59-cm ring-array diameter with eight uniformly spaced dipole elements operating over the frequency band 60–120 MHz [34]. The eight dipoles are fed as four active pairs of elements. There are four high-power amplifiers which drive the dipole pairs with up to 500 W average power per channel. Each of the four active channels has an electronically controlled variable-phase shifter for focusing the array. Temperature and electric-field probe sensors (both invasive and noninvasive) are used to monitor the treatment. A cool-water (5°–40°C) bolus between the patient and the phased array is used to prevent excess heating of the skin surface during the treatment. The bolus is filled with circulating deionized water, which has a very low RF propagation loss.

A candidate adaptive-nulling algorithm is a gradient search based on minimizing the signal received by electric-field sensors at the desired null positions while maintaining the signal amplitude at the focal point. The reason for considering this algorithm is that the BSD-2000 system measures the applied electric-field amplitude but not the phase. Note: the E-field probes used in the BSD-2000

---

<sup>1</sup>A similar movable multiapplicator phased array exists [12] and presumably could be modified to have adaptive capability.

**WATER  
BOLUS**



**DIPOLE PAIR**

<b>BSD MEDICAL CORP. MODEL BSD-2000</b>	
<b>OPERATING FREQ.</b>	<b>60-120 MHz</b>
<b>NO. CHANNELS</b>	<b>4</b>
<b>POWER</b>	<b>500 W/CHANNEL</b>
<b>ANTENNA</b>	<b>8-DIPOLE RING</b>

*Figure 1. A clinical hyperthermia phased-array antenna system (photograph courtesy of BSD Medical Corporation).*

system are short dipoles with semiconductor diode detectors [35-37]. A potentially better approach to performing adaptive hyperthermia is to use a channel-covariance-matrix-based algorithm and suitable transmit calibration to control the weights. If the electric-field phase and amplitude are measured (by modification of the E-field probe hardware to form in-phase and quadrature signals), the sample matrix inversion (SMI) algorithm [2] could be used to form the nulls. The concept of adaptive nulling as it applies to hyperthermia will now be described.

Recently, a technique called focused near-field adaptive nulling [38-44] has been investigated for testing the performance of radar and communications systems. A calibration probe antenna is used to focus the main beam at approximately one diameter  $D$  of the phased array. Additional (auxiliary) probe antennas are located in the sidelobe region of the phased-array quiescent-radiation pattern. Adaptive nulls are formed in the direction of these auxiliary probes. Computer simulations show that a radar system can be tested by using the focused near-field nulling technique [43]; experimental measurements of focused near-field adaptive nulling have been performed [44]. For the radar system, interference signals entering through uncontrolled sidelobes can reduce the signal-to-noise ratio (SNR); adaptive nulling [1] is commonly used to counteract this possible degradation. In the hyperthermia system, high transmit-antenna electric-field strengths can create hot spots in the target tissue. These high-temperature regions can possibly be alleviated with adaptive nulling of the electric field at specified positions on the surface of the target.

In the proposed adaptive hyperthermia concept, electric-field nulls are used to reduce the power delivered to potential hot spots. Computer simulations show that noninvasive electric-field probes can be used to eliminate hot spots that are interior to the phantom target tissue [3-6]. For example, an eight-element ring array with 60-cm diameter surrounding a transverse cross section at the prostate level is depicted in Figure 2(a). For computer simulation, the heterogeneous target is replaced with a homogeneous elliptical phantom. The transmit amplitude and phase of each element are assumed to be adaptively controlled so that a deep-seated tumor site receives maximum electric-field power while minimizing the electric-field power at four positions on the target surface as shown in Figure 2(b). Figure 3 summarizes the thermal simulation for a 120-MHz RF hyperthermia ring array with eight adaptively controlled dipole elements transmitting through a constant-temperature water bolus into a homogeneous elliptical target region. The tumor site is assumed to be at the center of the ellipse. The thermal distribution in Figure 3(a) contains two hot spots to the left and right of the focus. Note: a similar thermal distribution has been reported in the literature [12]. In Figure 3(b), adaptive nulling at four independent positions is in effect and the hot spots are eliminated.

Consider a potential clinical application of the proposed adaptive hyperthermia system with the BSD-2000 Sigma 60 system. The BSD-2000 hyperthermia system currently uses eight EP-400 noninvasive electric-field probes to monitor clinical hyperthermia treatments. The eight EP-400 probes (or eight EP-100 probes) could provide feedback signals to the adaptive algorithm. In theory, with four transmit channels three independent adaptive nulls can be formed using any three of the eight feedback signals. There are various methods to select the desired null sites. The adaptive algorithm could minimize the three largest measured electric field signals on the target

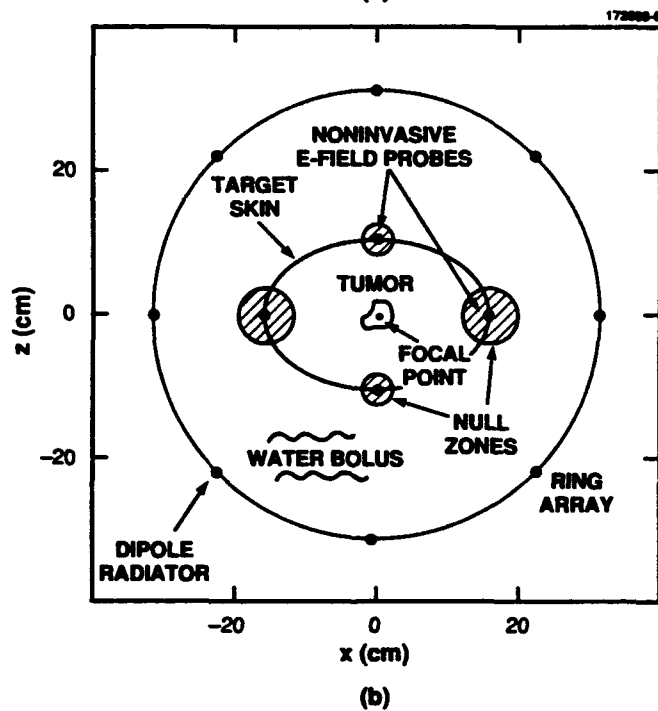
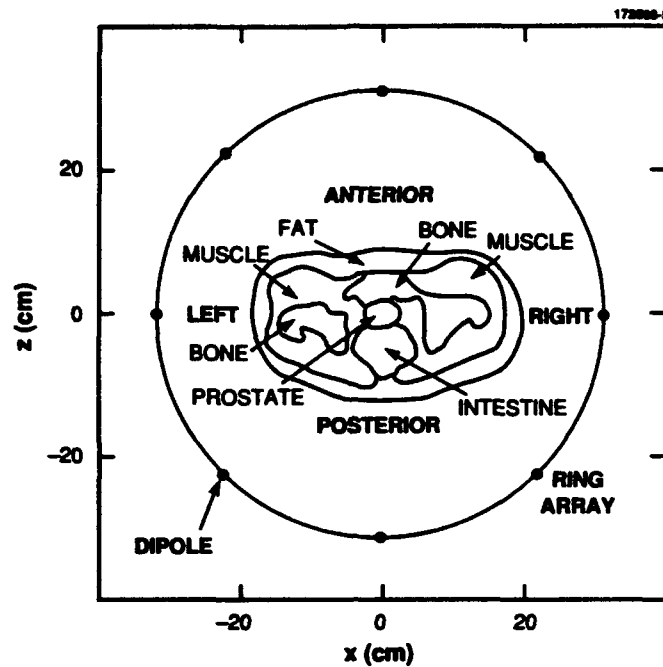


*Figure 2. (a) Transverse cross section at the prostate level. An eight-element hyperthermia ring array of dipole elements is used to irradiate a target body with sufficient power to elevate the tumor temperature in the target body to a therapeutic level. (b) Elliptical phantom target used to model the prostate (target)-level cross section. Shown are four noninvasive auxiliary E-field probes that are used in forming null zones with widths controlled by the individual null strengths. The null zones extend into the body to reduce the internal electric field at specified locations.*

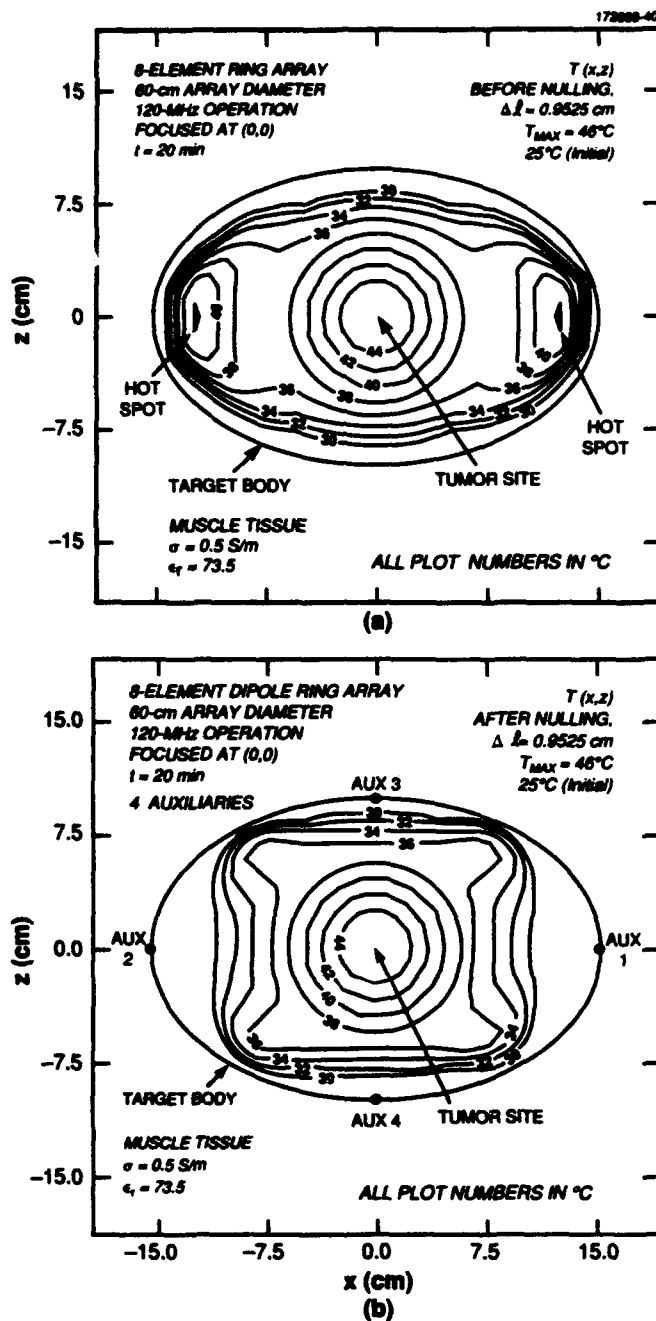


Figure 3. Simulated two-dimensional thermal pattern in elliptical phantom muscle-tissue target surrounded with  $10^{\circ}\text{C}$  constant-temperature water bolus. The incident RF power distribution is at 120 MHz and the initial temperature of the phantom is  $25^{\circ}\text{C}$ . Temperature contour levels are given in  $2^{\circ}\text{C}$  steps. (a) Before nulling; hot spots on the left and right sides of the target are present. (b) After nulling; hot spots are eliminated.

surface. If two or three positions are identified as potential hot spots, adaptive nulls could be automatically formed at those positions. Alternately, if during the heating therapy a patient can localize a painful tissue area, the nearest electric-field probe can be used as the feedback signal to the adaptive nulling algorithm. In some situations more than three independent adaptive nulls may be needed to produce a therapeutic thermal distribution. An extension of the present four-channel BSD-2000 system to eight channels would provide up to seven independent adaptive nulls plus a desired focus.

The remainder of this report is organized as follows. Section 2 discusses the concept for a noninvasive adaptive hyperthermia system and describes in detail the gradient-search feedback algorithm used in implementing the adaptive array. Section 3 describes the materials and methods used in obtaining the measured results. The phantom targets measured in this report are a saline-filled cylindrical phantom and a beef phantom. Section 4 gives measured results for an adaptive four-channel hyperthermia ring array operating at CW frequencies of 100 MHz and 120 MHz. The measured received RF-power distributions before and after adaptive nulling with short-dipole field probes are presented. Section 5 presents the conclusions.

## 2. THEORY

### 2.1 Noninvasive Adaptive Hyperthermia System Concept

The concept of a noninvasive adaptive-nulling hyperthermia system [3-6] is shown in Figure 4. Theoretically, to generate the desired field distribution in a clinical adaptive hyperthermia system, receiving sensors are positioned as close as possible to the focus (tumor site) and where high temperatures are to be avoided (such as near the spinal cord and scar tissue). A noninvasive adaptive nulling system is achieved by placing auxiliary sensors  $1, 2, \dots, N_{aux}$  on the target skin as shown. The null zones centered at each auxiliary probe naturally extend into the elliptical target region to eliminate undesired hot spots. The width of each null zone is directly related to the strength of each null. The strength of each null (sometimes referred to as the amount of cancellation) is directly related to the SNR at the sensor position. A low SNR produces a small amount of nulling, a high SNR a large amount of nulling. The resolution or minimum spacing between the focus and null positions is normally equal to the half-power beamwidth of the antenna. The resolution is enhanced somewhat by using weak nulls whenever the separation between the null and focus is closer than the half-power beamwidth. The half-power angular beamwidth of an antenna aperture with diameter  $D$  in wavelengths is approximated by

$$\theta_{HPBW} = \frac{\lambda}{D} \quad (1)$$

where  $\lambda$  is the wavelength. The antenna half-power focal beamwidth (spot size) in units of length is expressed as

$$s = \theta_{HPBW} \times R \quad (2)$$

where  $R$  is the focal distance of the antenna. Using Equation (1) and substituting  $R = D/2$  for a ring array focused at the origin in Equation (2) yields

$$s = \frac{\lambda}{2} \quad (3)$$

Thus, the focal spot size or resolution of a ring array is one-half the wavelength in the target body.

Initially, the hyperthermia array is focused to produce the required field intensity at the tumor. An invasive probe is required to achieve the optimum focus at depth. To avoid hot spots, it is necessary to minimize the power received at the desired null positions and to constrain the array weights to deliver a required amount of transmitted or focal-region power. The adaptive array weights (with gain  $g$  and phase  $\phi$ ) are controlled by either the SMI algorithm or a gradient-search algorithm to rapidly form the nulls before a significant amount of target heating takes place. With

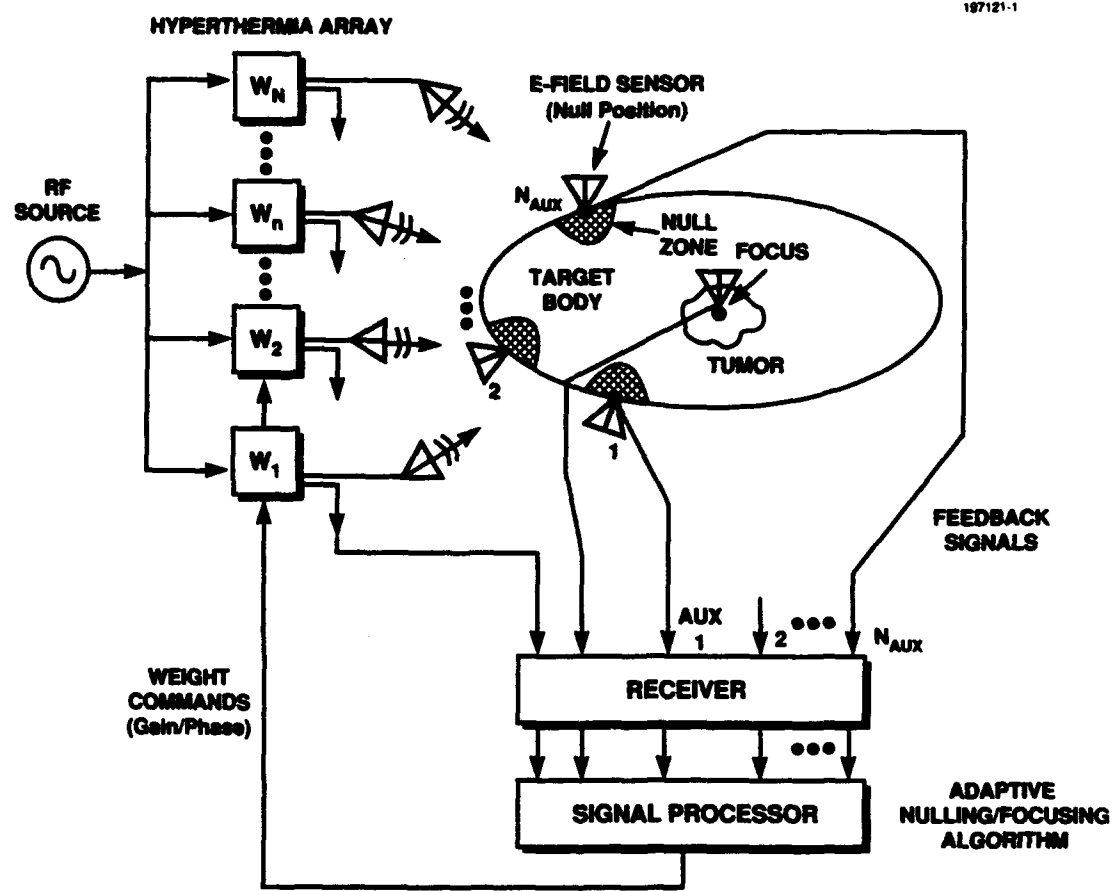


Figure 4. Noninvasive adaptive hyperthermia system concept.

this adaptive technique, it should be possible to avoid hot spots and maintain a therapeutic thermal dose distribution at the tumor.

## 2.2 Adaptive Transmit-Array Formulation

Consider a hyperthermia array with  $N$  identical antenna elements. Note:  $N$  will represent  $N$  pairs of identical antenna elements for the BSD-2000 system. The input signal to each of the  $N$  array elements is obtained from the weighted signal distributed by a power divider network. The number of adaptive channels is denoted  $N$ . Let  $\mathbf{w} = (w_1, w_2, \dots, w_N)^T$  denote the adaptive channel weight vector as shown in Figure 4. (Superscript  $T$  means transpose.)

For an adaptive annular array focused at the origin in homogeneous tissue, the normalized quiescent weight vector is simply  $\mathbf{w}_q = (1, 1, 1, \dots, 1)^T$ ; that is, the amplitude and phase illumination are uniform. Commonly, the weight vector is constrained to deliver a required amount of power to the hyperthermia array or to the tumor. For simplicity in the experimental adaptive-hyperthermia-array control software, the weights are constrained such that

$$\sum_{n=1}^N |w_n| = K \quad , \quad (4)$$

where  $|w_n|$  is the transmit-weight amplitude for the  $n$ th adaptive channel and  $K$  is a constant. To generate adaptive nulls, the transmit weights (phase and gain) are controlled by either the SMI algorithm or a gradient-search algorithm. The SMI algorithm has the flexibility to operate in either open- or closed-loop feedback modes [45]; the gradient-search algorithm operates only in a feedback mode.

### 2.2.1 Gradient-Search Algorithm

Gradient-search algorithms are commonly used in adaptive-array applications where the channel correlation cannot be calculated or measured. With a gradient search, only the output power of the receiver channels needs to be measured and is used as a feedback signal to the algorithm. A wide variety of gradient searches exist [46-50].

Under conditions where only the probe-received power is measured (as in the BSD-2000 system), it is appropriate to consider a gradient-search algorithm to minimize the E-field power at selected positions. The gradient search is used to control the transmit weights iteratively so that the RF signal received by the probe array is minimized. The transmit-array weights (gain and phase) are adaptively changed in small increments and the probe-array output power is monitored to determine weight settings that reduce the output power most rapidly to a null. The mathematical formulation for the gradient search is developed in a straightforward manner [50, 51] and will now be described in the context of hyperthermia. Although the mathematical formulation is given as a minimization problem, the equations are readily converted to the maximization problem.

The summation of power received at the electric-field probes is denoted by  $p^{rec}$ . The adaptive array cancellation ratio, denoted  $C$ , is defined here as the ratio of the summation of probe-received power after adaption  $p_a$  to the summation of probe-received power before adaption  $p_b$ ; that is,

$$C = \frac{p_a}{p_b} \quad (5)$$

Consider now  $J$  sets (or iterations) of  $N$  transmit weights that are applied to an adaptive hyperthermia phased-array antenna. In terms of adaptive nulling, the optimum transmit-weight settings (from the collection of  $J$  sets of  $N$  transmit weights) occur when the total interference power received by the auxiliary probe array, denoted  $p^{rec}$ , is minimized. For notational convenience let a figure of merit  $F$  denote  $p^{rec}$  and employ a method of steepest-descent gradient search to find the optimum transmit weights to minimize  $F$ ; that is,

$$F_{opt} = \min(F_j) \quad j = 1, 2, \dots, J \quad (6)$$

Assume that there are  $N$  complex transmit weights in the hyperthermia phased array as suggested by the amplitude and phase scatter diagram depicted in Figure 5. The  $n$ th transmit weight in the  $j$ th configuration (or iteration) of transmit weights is denoted

$$w_{nj} = A_{nj}e^{j\Phi_{nj}} \quad (7)$$

where  $A_{nj}$  is the transmit-weight amplitude distributed over the range  $A_{min}$  to  $A_{max}$  and  $\Phi_{nj}$  is the transmit-weight phase distributed over the range  $\Phi_{min}$  to  $\Phi_{max}$ . The goal is to find the values of amplitude and phase for each of the  $N$  transmit weights such that the figure of merit ( $p^{rec}$ ) is minimized. When the figure of merit is minimized, adaptive radiation pattern nulls will be formed at the auxiliary sensor positions.

Assuming an initial setting of the  $N$  transmit weights, the weights are adjusted by dithering them until the optimum figure of merit is achieved. The goal is to find the collective search directions for the  $N$  transmit weights such that  $F$  decreases most rapidly; that is, transmit weights are selected so that the directional derivative is minimized at  $(\mathbf{A}_j, \mathbf{\Phi}_j)$ , where  $\mathbf{A}_j$  and  $\mathbf{\Phi}_j$  are the amplitude and phase column vectors, respectively.

The directional derivative of  $F_j$  is expressed in terms of the amplitude and phase changes of the transmit weights as

$$D(F_j) = \sum_{n=1}^N \left( \frac{\partial F_j}{\partial A_{nj}} r_{A_{nj}} + \frac{\partial F_j}{\partial \Phi_{nj}} r_{\Phi_{nj}} \right) \quad (8)$$

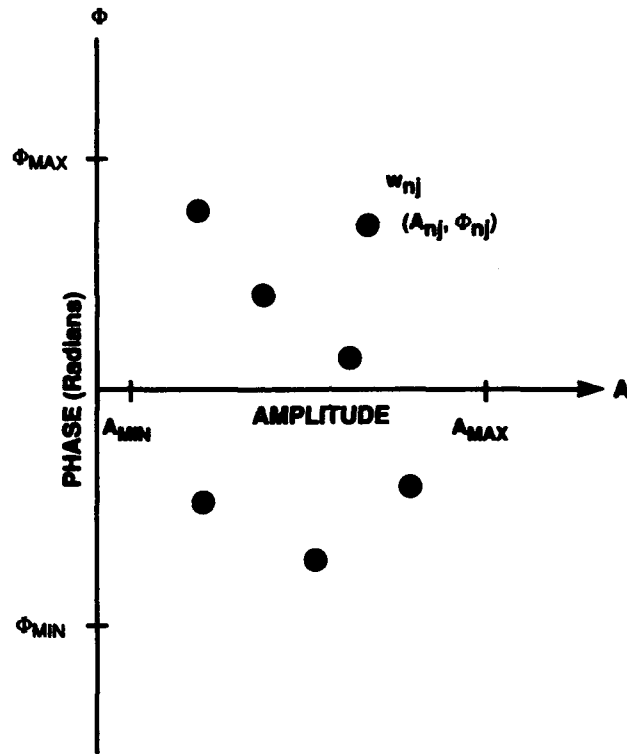


Figure 5. Scatter diagram in rectangular coordinates for the amplitude and phase of the transmit weights in a hyperthermia phased-array antenna. The  $n$ th transmit weight in the  $j$ th configuration of transmit weights is denoted  $w_{nj}$ .

where  $\partial$  means partial derivative and  $r_{A_{nj}}, r_{\Phi_{nj}}$  are the  $(A, \Phi)$  directions for which  $F_j$  is decreasing most rapidly. The directions  $r_{A_{nj}}, r_{\Phi_{nj}}$  are constrained by

$$\sum_{n=1}^N (r_{A_{nj}}^2 + r_{\Phi_{nj}}^2) = 1 \quad (9)$$

The goal is to minimize  $D(F_j)$  subject to the above constraint equation.

Using Lagrange multipliers, construct the Lagrangian function

$$L_j = \sum_{n=1}^N \left( \frac{\partial F_j}{\partial A_{nj}} r_{A_{nj}} + \frac{\partial F_j}{\partial \Phi_{nj}} r_{\Phi_{nj}} \right) + G \left[ 1 - \sum_{n=1}^N (r_{A_{nj}}^2 + r_{\Phi_{nj}}^2) \right] \quad (10)$$

where  $G$  is a constant to be determined. The requirement that  $L_j$  be an extremum implies

$$\frac{\partial L_j}{\partial r_{A_{nj}}} = \frac{\partial F_j}{\partial A_{nj}} - 2Gr_{A_{nj}} = 0, \quad n = 1, 2, \dots, N \quad (11)$$

$$\frac{\partial L_j}{\partial r_{\Phi_{nj}}} = \frac{\partial F_j}{\partial \Phi_{nj}} - 2Gr_{\Phi_{nj}} = 0, \quad n = 1, 2, \dots, N \quad (12)$$

or

$$r_{A_{nj}} = \frac{1}{2G} \frac{\partial F_j}{\partial A_{nj}} \quad (13)$$

$$r_{\Phi_{nj}} = \frac{1}{2G} \frac{\partial F_j}{\partial \Phi_{nj}} \quad (14)$$

Squaring Equations (13) and (14) and invoking Equation (9) yields

$$\sum_{n=1}^N (r_{A_{nj}}^2 + r_{\Phi_{nj}}^2) = 1 = \frac{1}{4G^2} \sum_{n=1}^N \left[ \left( \frac{\partial F_j}{\partial A_{nj}} \right)^2 + \left( \frac{\partial F_j}{\partial \Phi_{nj}} \right)^2 \right] \quad (15)$$

thus,

$$G = \pm \frac{1}{2} \sqrt{\sum_{n=1}^N \left[ \left( \frac{\partial F_j}{\partial A_{nj}} \right)^2 + \left( \frac{\partial F_j}{\partial \Phi_{nj}} \right)^2 \right]} \quad (16)$$

Substituting Equation (16) into Equations (13) and (14) gives

$$r_{A_{nj}} = - \frac{\frac{\partial F_j}{\partial A_{nj}}}{\sqrt{\sum_{n=1}^N \left[ \left( \frac{\partial F_j}{\partial A_{nj}} \right)^2 + \left( \frac{\partial F_j}{\partial \Phi_{nj}} \right)^2 \right]}} \quad (17)$$

$$r_{\Phi_{nj}} = - \frac{\frac{\partial F_j}{\partial \Phi_{nj}}}{\sqrt{\sum_{n=1}^N \left[ \left( \frac{\partial F_j}{\partial A_{nj}} \right)^2 + \left( \frac{\partial F_j}{\partial \Phi_{nj}} \right)^2 \right]}} \quad (18)$$

In Equations (17) and (18) the minus sign was chosen corresponding to the direction of maximum function decrease. (Note: by changing the minus sign to a plus sign in Equations (17) and (18), the search directions then correspond to the direction of maximum function increase, i.e., the plus sign is used to maximize the power delivered to the focus or tumor site.) The partial derivatives

$$\frac{\partial F_j}{\partial A_{nj}}, \frac{\partial F_j}{\partial \Phi_{nj}} ; n = 1, 2, \dots, N \quad (19)$$

represent the gradient directions for maximum function decrease.

Because the figure of merit  $F$  is measured and cannot be expressed in analytical form, the partial derivatives are numerically evaluated using finite differences. Thus,

$$\frac{\partial F_j}{\partial A_{nj}} = \frac{\Delta F_{A_{nj}}}{2\Delta A_{nj}} \quad (20)$$

$$\frac{\partial F_j}{\partial \Phi_{nj}} = \frac{\Delta F_{\Phi_{nj}}}{2\Delta \Phi_{nj}} \quad (21)$$

where, as shown in Figure 6,

$$\Delta F_{A_{nj}} = F_j(A_{nj} + \Delta A_{nj}; \Phi_{nj}) - F_j(A_{nj} - \Delta A_{nj}; \Phi_{nj}) \quad (22)$$

$$\Delta F_{\Phi_{nj}} = F_j(A_{nj}; \Phi_{nj} + \Delta \Phi_{nj}) - F_j(A_{nj}; \Phi_{nj} - \Delta \Phi_{nj}) \quad (23)$$

and  $\Delta A_{nj}$  and  $\Delta \Phi_{nj}$  are the maximum step sizes. Assume for now that the increments  $\Delta A_{nj}$  and  $\Delta \Phi_{nj}$  depend on the iteration number  $j$  and transmit element index  $n$ . Substituting Equations (20) and (21) into Equations (17) and (18) gives the desired result for the search directions

$$r_{A_{nj}} = -\frac{\frac{\Delta F_{A_{nj}}}{\Delta A_{nj}}}{\sqrt{\sum_{n=1}^N \left[ \left( \frac{\Delta F_{A_{nj}}}{\Delta A_{nj}} \right)^2 + \left( \frac{\Delta F_{\Phi_{nj}}}{\Delta \Phi_{nj}} \right)^2 \right]}} \quad (24)$$

$$r_{\Phi_{nj}} = -\frac{\frac{\Delta F_{\Phi_{nj}}}{\Delta \Phi_{nj}}}{\sqrt{\sum_{n=1}^N \left[ \left( \frac{\Delta F_{A_{nj}}}{\Delta A_{nj}} \right)^2 + \left( \frac{\Delta F_{\Phi_{nj}}}{\Delta \Phi_{nj}} \right)^2 \right]}} \quad (25)$$

The new amplitude and phase settings of the  $(j+1)$ th transmit-weight configuration are computed according to

$$A_{n,j+1} = A_{nj} + \Delta A_{nj} r_{A_{nj}} \quad (26)$$

$$\Phi_{n,j+1} = \Phi_{nj} + \Delta \Phi_{nj} r_{\Phi_{nj}} \quad (27)$$

For the current software implementation of the gradient search in these experiments, assume (for convenience) that the step sizes are independent of both the iteration number and the adaptive channel number; that is,

$$\Delta A_{nj} = \Delta A \quad (28)$$

$$\Delta \Phi_{nj} = \Delta \Phi \quad (29)$$

In some situations it may be desirable to change the step size at each iteration as considered in Farina and Flam [46], but that possibility has not been explored in these measurements.

### 2.3 System Considerations

Figure 7 shows a block diagram for an adaptive hyperthermia system controlled by the gradient-search algorithm. The transmit weights  $w_{1j}, \dots, w_{nj}, \dots, w_{Nj}$  at the  $j$ th iteration are shown at the top of the figure. The transmit phased-array antenna induces a voltage across the terminals of the  $i$ th receive field probe antenna. For any given configuration of the transmit weights, each weight is dithered by a small amount in amplitude and phase and the received powers at the

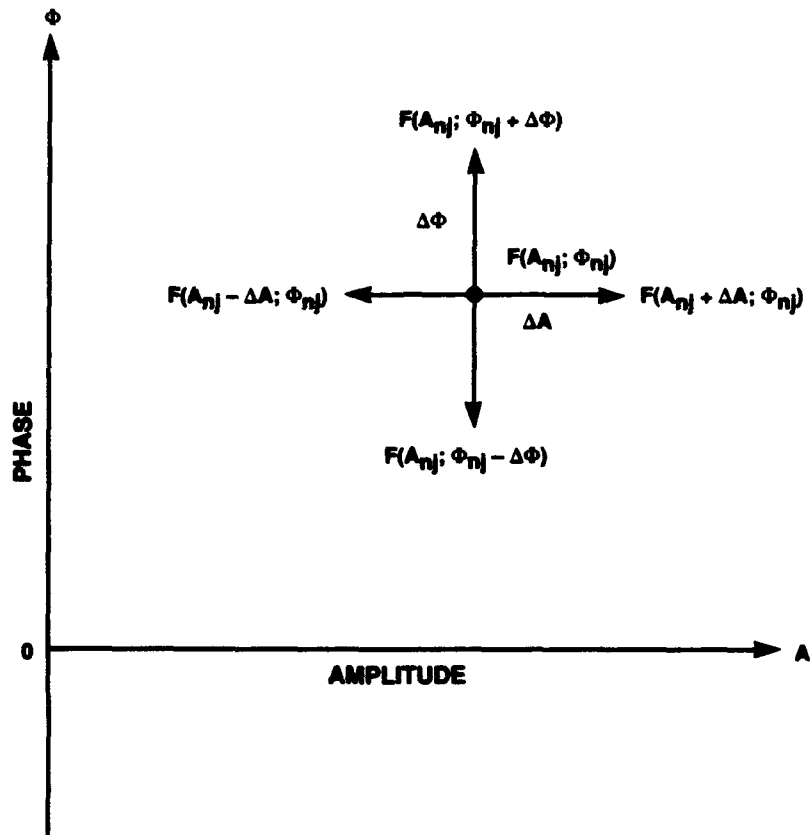


Figure 6. Figure of merit with transmit-weight dithering for optimum search directions.

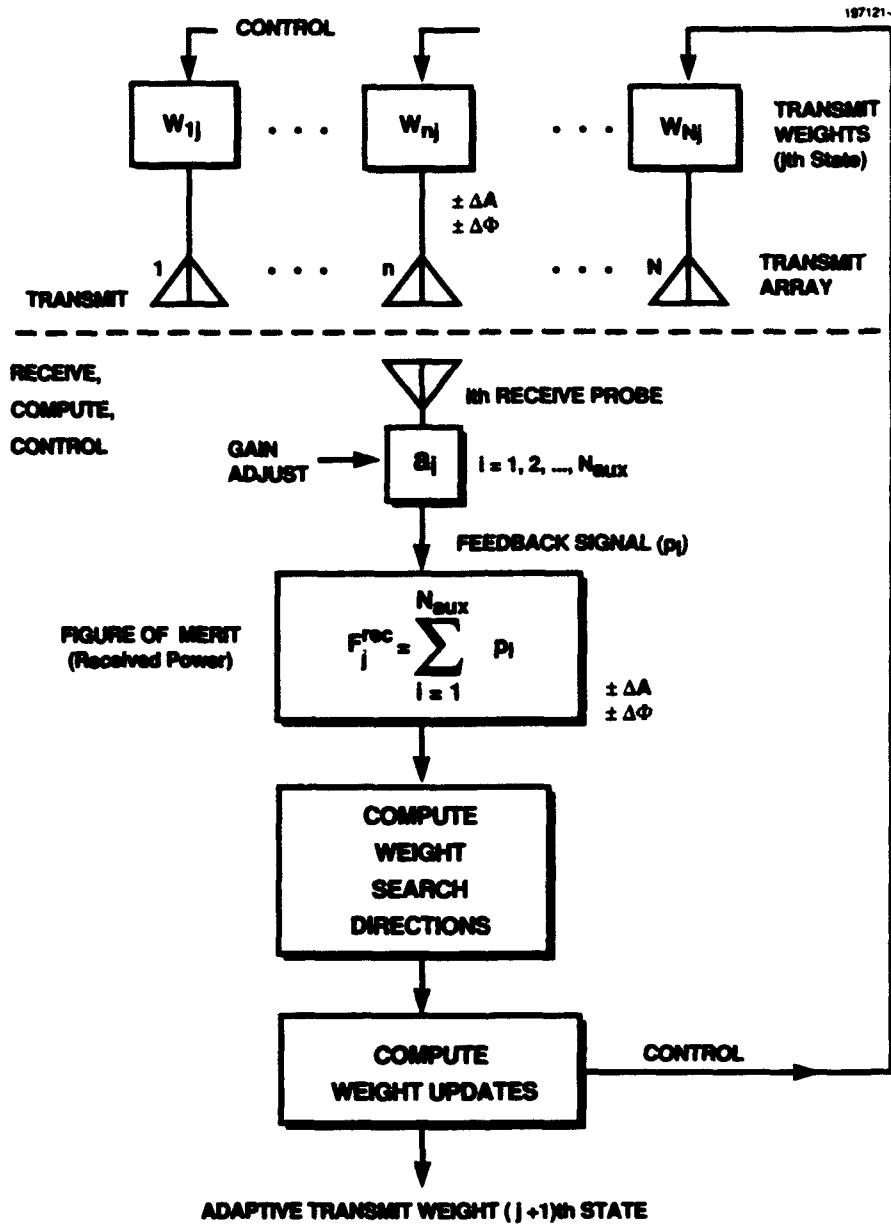


Figure 7. Gradient-search algorithm block diagram for adaptive-nulling hyperthermia system.

electric-field probes are stored in the computer for calculation of the figure of merit, search directions, and updated  $(j + 1)$ th transmit-weight configuration. The weight dithering of one transmit weight must be done with the remaining transmit weights in their  $j$ th state. The figure of merit  $F_j$  in the adaptive hyperthermia system is the power received by the auxiliary probe array, as indicated in the block diagram. The figure of merit is a rectangular matrix with dimensions  $(N \times 4)$ . A dimensionality of four is due to the plus and minus dithering of both amplitude and phase. Search directions for the adaptive transmit weights are based on minimizing the auxiliary-probe-array received power and are computed based on Equations (24) and (25). The transmit weights for the next configuration  $(j + 1)$  are computed from Equations (26) and (27). The adaptive weight vector  $w_a$  is achieved when the  $(j + 1)$ th weight configuration has converged. Based on computer simulations not shown here, convergence occurs in less than one hundred iterations, depending on the step sizes  $(\Delta A$  and  $\Delta \Phi)$  and number of adaptive null positions  $N_{aux}$ .

### 3. MATERIALS AND METHODS

The hyperthermia phased-array system used in these measurements is the BSD Medical Corporation Model BSD-2000 with Sigma-60 applicator. The applicator has a 59-cm array diameter with eight uniformly spaced dipole elements (dipole length is 44 cm) operating over the frequency band 60–120 MHz [34]. The eight dipoles are fed as four active pairs of elements with up to 500 W average power per channel. Each of the four active channels has an electronically controlled variable-phase shifter for phase focusing the array. The variable transmit gain and phase modules are controlled by digital to analog (D/A) converters. Temperature and electric-field probe sensors (both invasive and noninvasive) are used to monitor the treatment. The bolus is filled with circulating deionized water, which has a very low RF propagation loss. A photograph of the SUNY Health Science Center Hyperthermia Treatment Facility is shown in Figure 8. The hyperthermia array is controlled and monitored by a PDOS-based computer system and the array applicator is located in an RF-shielded room. Figure 9 shows the Sigma-60 ring-array applicator, which can be moved by hand to the desired longitudinal position on the patient-support assembly. A photograph of the four-channel RF transmitter rack is shown in Figure 10. Figure 11 shows the coaxial RF transmit feed lines for the dipole array.

Three models of electric-field probes are used in these measurements. For invasive electric-field measurements, a BSD Model EP-500 probe is used. For noninvasive electric-field measurements, BSD Model Numbers EP-100 and EP-400 are used. The design of the EP-500 probe is as follows [37]: The short metallic leads of a Schottky diode are connected between two highly resistive conductive leads. A 1-cm length of conducting wire is added to one of the resistive leads and responds to linear polarization. The leads of the diode and the additional conducting wire act as an offset-feed dipole antenna. The lengths of the dipole antennas used in the above three probes are as follows: EP-500 is a 1-cm dipole, EP-100 is a 3-cm dipole, and EP-400 is a 3-element array of dipoles with a total length of 23 cm. Two Bowman temperature probes (provided with the BSD-2000 system) are used to monitor the beef phantom temperatures. In this report, assume that an EP-100 probe will provide localized adaptive nulls; thus, the EP-100 probe is used for providing the feedback signals.<sup>2</sup>

The saline-filled (0.9% NaCl in deionized water) cylindrical phantom (28-cm diameter and 40-cm length), located on the patient-support sling, is shown in Figure 12. Note: the cylindrical phantom is a 6-gallon polyethylene bottle. In this figure, a dipole probe is mounted on the surface of the phantom and is connected to the temperature/electric-field monitoring unit.

The beef phantom used in these experiments, depicted in Figure 13, is a tapered cut obtained from the hind leg just above the knee. The front face of the beef has a horizontal width of 38 cm

---

<sup>2</sup>The EP-400 field probes have also been used for feedback signals and the measured null strengths are similar to the EP-100 measured data presented in this report.

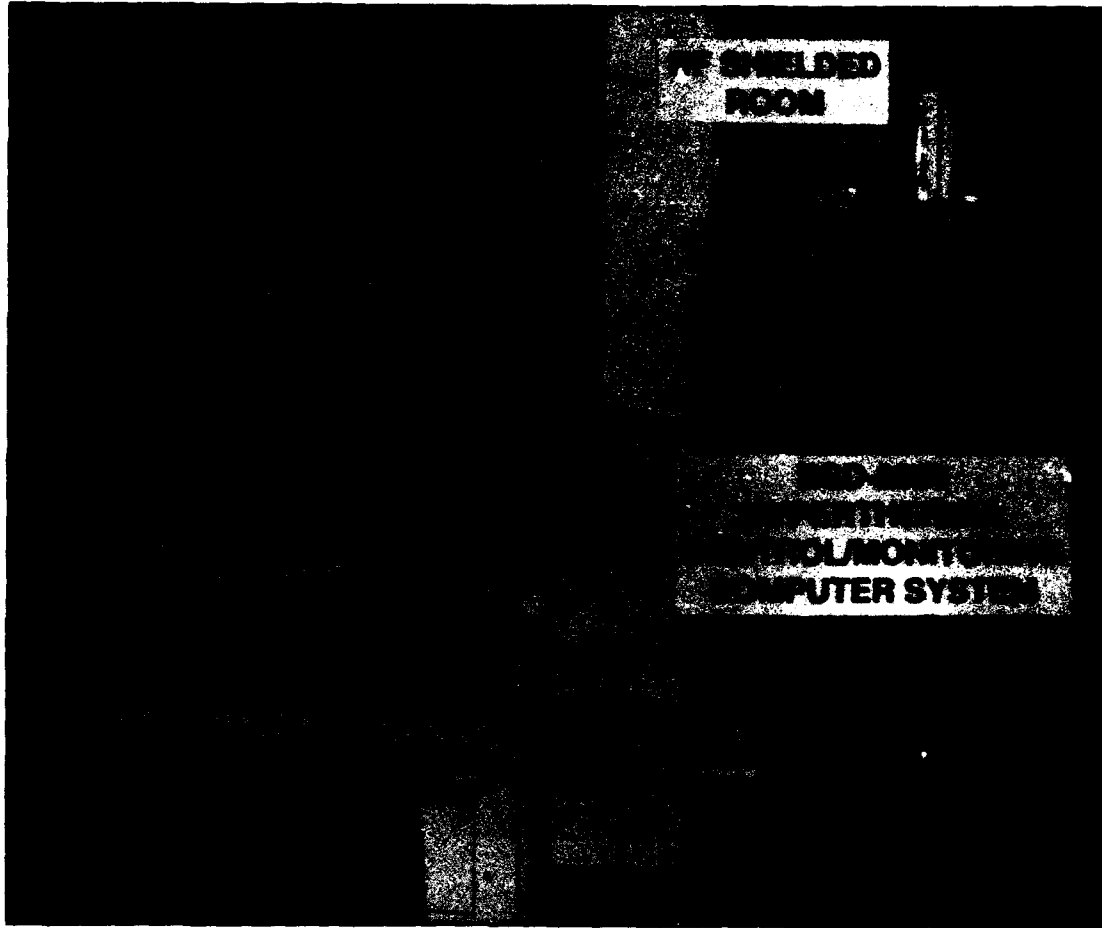


*Figure 8. Hyperthermia treatment facility at the Health Science Center, State University of New York.*

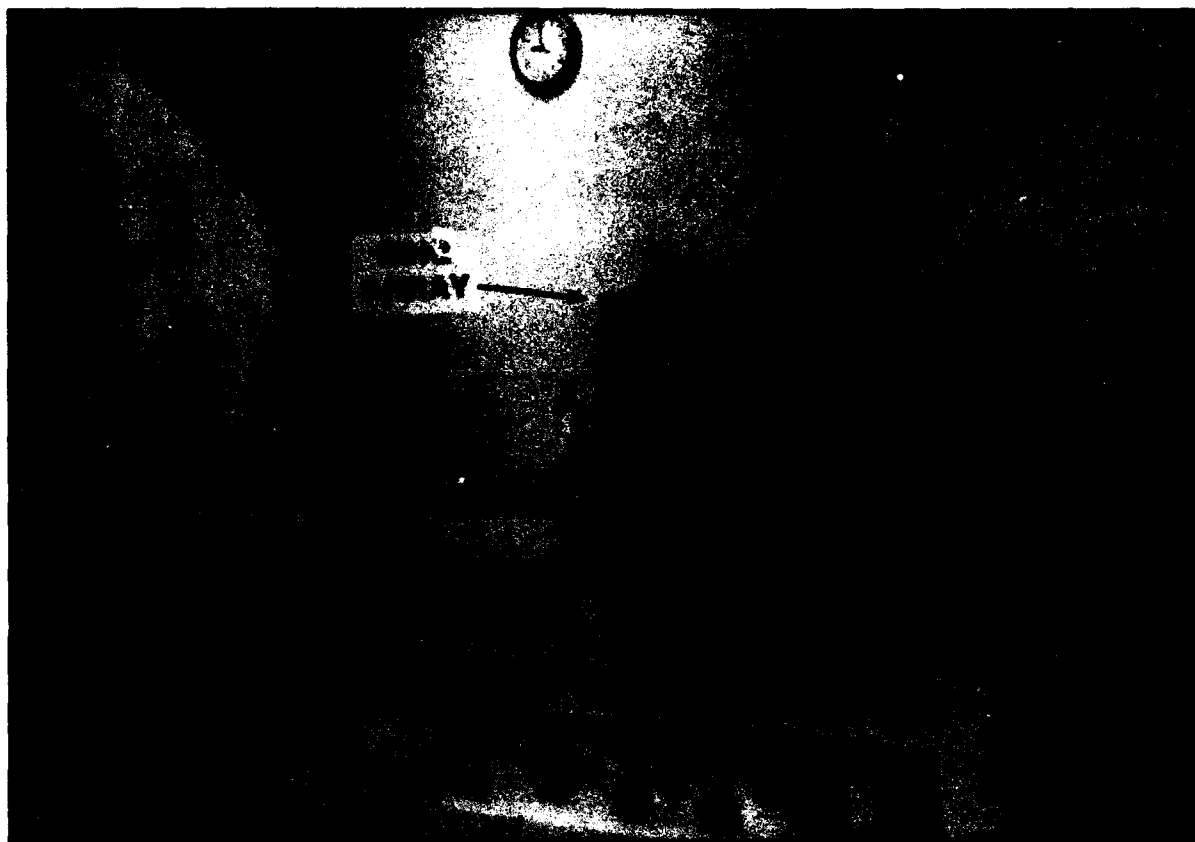


*Figure 9. BSD-2000 Sigma-60 applicator on patient-support assembly at SUNY.*

107121-7



*Figure 10. BSD-2000 transmitter rack.*



*Figure 11. BSD-2000 Sigma-60 applicator with coaxial feedlines.*

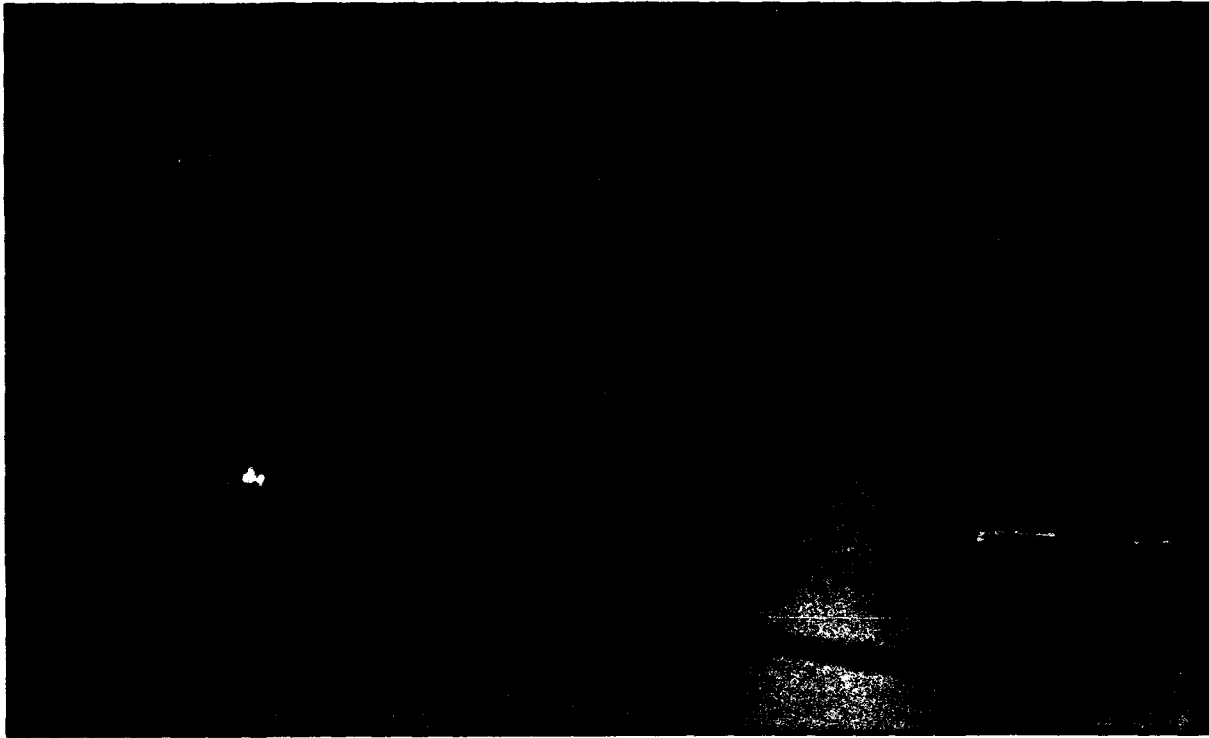


*Figure 12. Saline-filled cylindrical phantom with dipole probe and temperature/electric-field monitoring unit.*

and a vertical height of 23 cm. The thickness of the beef is 15 cm and the weight is 10.9 kg. The probe positions used in the experiments are indicated.

The estimated dielectric properties of the various materials used in these experiments are given in Table 1.

**TABLE 1**  
**Dielectric Properties of Materials Used in the Experiments**

<b>Material</b>	<b>Relative Dielectric Constant</b>	<b>Electrical Conductivity</b>
Deionized Water	78.0	0.0001
0.9 % NaCl Phantom	75.0	1.5
Polyethylene	2.25	0.0002
Beef Tissue	50.0	1.0
Fat	7.5	0.067
Bone	7.5	0.067

A computer program that implements the gradient-search algorithm was developed by MIT Lincoln Laboratory and integrated with the BSD Medical Corporation quad-amplifier control and temperature/electric-field monitoring software at SUNY. The MIT/SUNY integrated software allows the user to run either adaptive-nulling or adaptive-focusing algorithms and to monitor the output power of the electric-field probes during the gradient search. The software also writes measured data to a file. The adaptive-nulling algorithm uses phase and amplitude control to form the nulls—the adaptive-focusing algorithm uses only phase control to maximize the focal-point electric field.

● ELECTRIC-FIELD PROBE SITES  
X TEMPERATURE PROBE SITES  
FRONT FACE VIEW

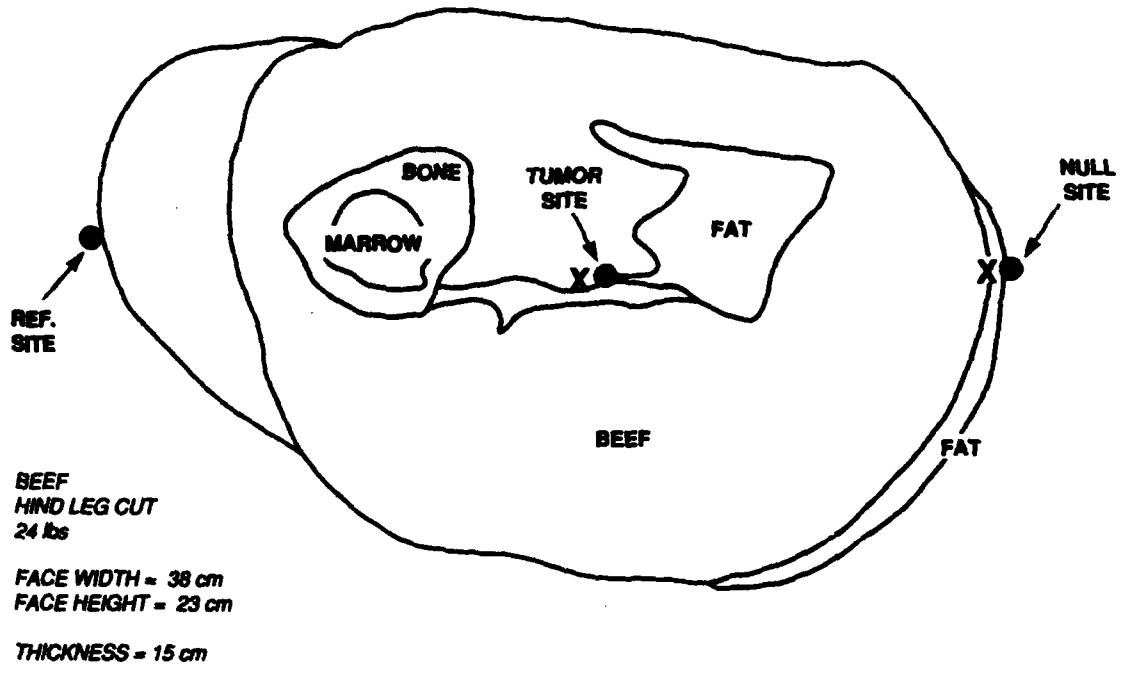


Figure 13. Front face dimensions and probe positions for beef phantom.

## 4. MEASURED RESULTS

In this section, measured data are presented for the saline-filled cylindrical-phantom and beef-phantom targets. Measurement frequencies were 100 MHz for the cylindrical phantom and 120 MHz for the beef phantom. These frequencies were selected by monitoring the reflected power level of the transmitter channels as a function of frequency. Frequencies where the reflected power is low were determined by trial and error.

The experimental test setup for the saline-filled cylindrical phantom is shown in Figure 14. Three electric-field probes are used to monitor the electric-field distribution. One probe is mounted invasively at the center of the cylindrical phantom and two probes are mounted on the left and right sides of the phantom. The power measured at the invasive probe site is taken as the power delivered to a fictitious tumor site.

The experimental test setup for the beef phantom is shown in Figure 15. Three electric-field probes are used to monitor the electric-field distribution. One probe is mounted invasively at the center of the beef phantom and two probes are mounted on the left and right sides of the phantom. The power measured at the invasive probe site is taken as the power delivered to a fictitious tumor site.

For the first experiment, one adaptive null is formed on the right side of the cylindrical phantom while the electric field is monitored at the center and left side of the phantom. In the second experiment, two adaptive nulls are formed independently on the left and right sides of the cylindrical phantom while monitoring the tumor-site power. The longitudinal characteristics of one of the adaptive nulls is quantified by measurement. In the third experiment, an adaptive focusing gradient search was run for the cylindrical phantom. The focus was positioned on the surface of the phantom. In the fourth experiment, one adaptive null on the side of the beef is measured. Thermocouple data are presented for this case.

The appendix lists the raw A/D data for the measured electric-field probe powers in the phantom experiments. In the following sections, the A/D converter data is converted to power in dB by computing  $10 \log(p)$  where  $p$  is the value (measured power) of the A/D converter.

### 4.1 One Adaptive Null for Cylindrical Phantom

The invasive EP-500 probe is mounted in the center of the cylindrical phantom and measures the electric-field power at the simulated tumor site. The probe is inserted in a catheter through the rubber plug on top of the phantom. An EP-400 probe is taped to the left side of the phantom and an EP-100 probe is taped to the right side of the phantom. The EP-400 probe measures a reference electric field, while the EP-100 measures the adaptive-nulling feedback signal. A 50-iteration adaptive-nulling gradient search was executed for this test configuration at 100 MHz. The gradient-search step sizes in terms of raw D/A converter states are  $\Delta A = 10$  and  $\Delta \Phi = 50$ . Note: the D/A converters have 12 bits, thus 4096 states. The commanded initial transmit-weight amplitude

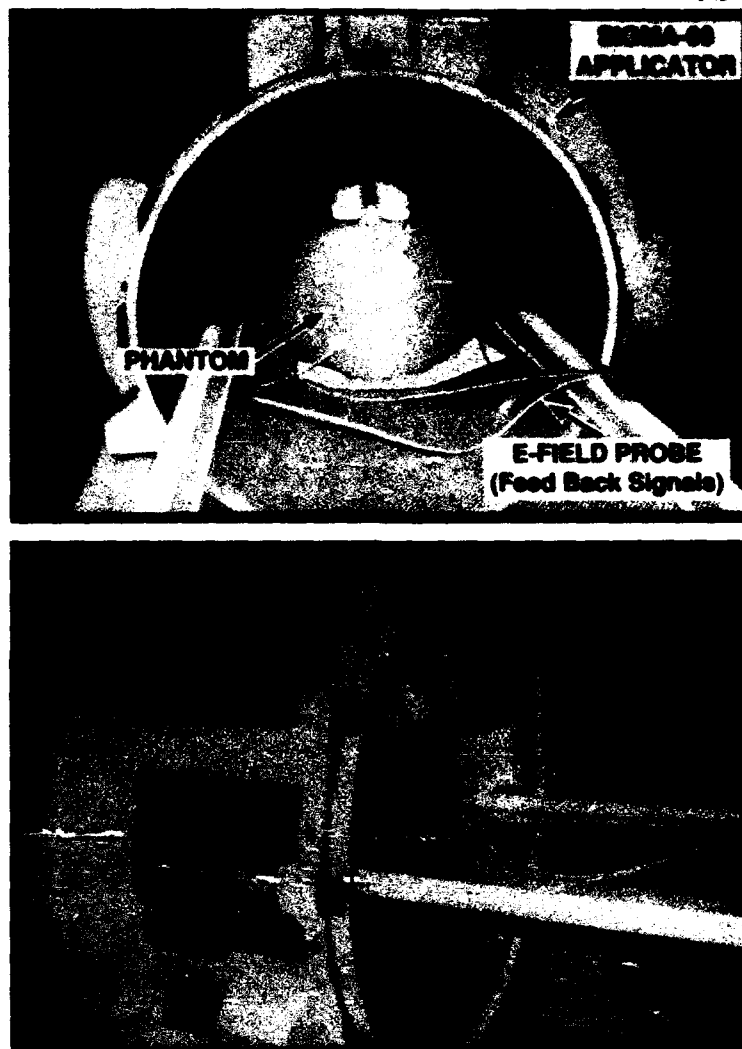


*Figure 14. Experimental test setup for the saline-filled cylindrical phantom. Three probes are used to monitor the electric field during the adaptive-nulling measurements.*

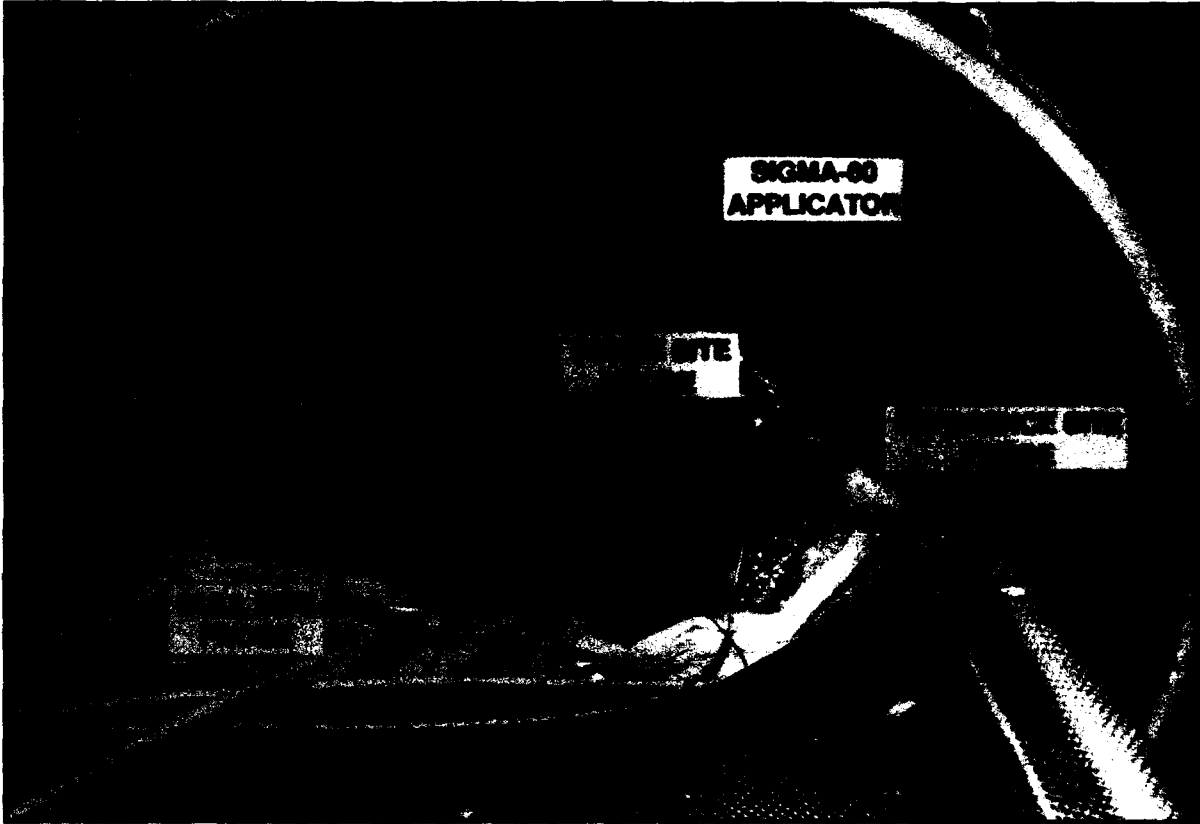


*Figure 15. Beef phantom target with electric-field probes and thermocouples.*

states on channels 1 to 4 <sup>3</sup> are (commanded D/A states: 500, 500, 500, 500) or (forward power in watts: 215 W, 215 W, 215 W, 215 W) <sup>4</sup> and the corresponding phase states are (commanded D/A states: 500, 500, 500, 500) or (equivalent phase lag: 89°, 89°, 89°, 89°). After 50 iterations of the nulling algorithm, the transmit-amplitude states are (commanded D/A states: 620, 668, 417, 294) or (forward power in watts: 370 W, 440 W, 98 W, 8 W) and the phase states are (commanded D/A states: 58, 578, 594, 664) or (equivalent phase lag: 45°, 94°, 95°, 99°). The measured electric field as a function of iteration number is displayed in Figure 16. There are three curves plotted; each curve is normalized to 0 dB at the initial iteration. The null-site probe power clearly decreases during the first 40 iterations. After 44 iterations, the average null-site amplitude (cancellation) is about -20 dB. The tumor site power has dropped by about 5 dB at iteration 50; this power reduction is attributed in part to the beam peak shifting away from the focus. The reference-site power stays relatively constant during the 50 iterations.

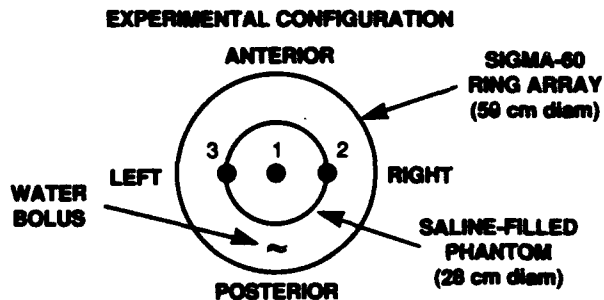
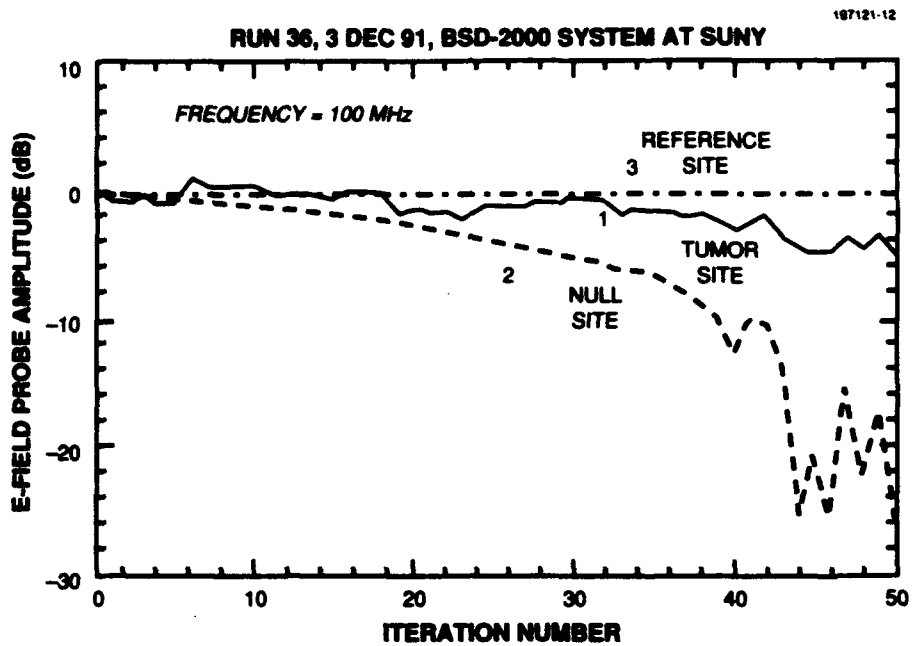
#### 4.2 Two Adaptive Nulls for Cylindrical Phantom

The second experiment involves forming two simultaneous adaptive nulls. The invasive EP-500 probe is mounted in the center of the cylindrical phantom and measures the electric-field power at the simulated tumor site. Two EP-100 probes are taped to the left and right sides of the phantom and measure the adaptive-nulling feedback signals. A 50-iteration adaptive-nulling gradient search was executed for this test configuration at 100 MHz. As before, the gradient-search step sizes in terms of raw D/A converter states are  $\Delta A = 10$  and  $\Delta \Phi = 50$ . The initial transmit-weight amplitude states on channels 1 to 4 are (commanded D/A states: 500, 500, 500, 500) or (forward power in watts: 215 W, 215 W, 215 W, 215 W) and the corresponding phase states are (commanded D/A states: 500, 500, 500, 500) or (equivalent phase lag: 89°, 89°, 89°, 89°). After 50 iterations of the nulling algorithm, the transmit-amplitude states are (commanded D/A states: 744, 379, 482, 396) or (forward power in watts: 510 W, 55 W, 190 W, 76 W) and the corresponding phase states are (commanded D/A states: 1, 676, 228, 781) or (equivalent phase lag: 0°, 99°, 58°, 101°). The measured electric field as a function of iteration number is displayed in Figure 17. The two null-site probe powers decrease nearly monotonically over the 50 iterations. At iteration 50, the cancellation for null-site probe #2 is -18.0 dB, while the cancellation for null-site probe #3 is -11.5 dB. The tumor-site probe power stays relatively constant during the 50 iterations. With the two symmetric nulls, the main beam tends to stay centered at the desired focus [3].

---

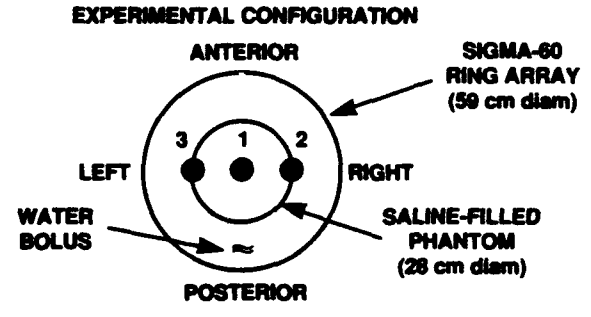
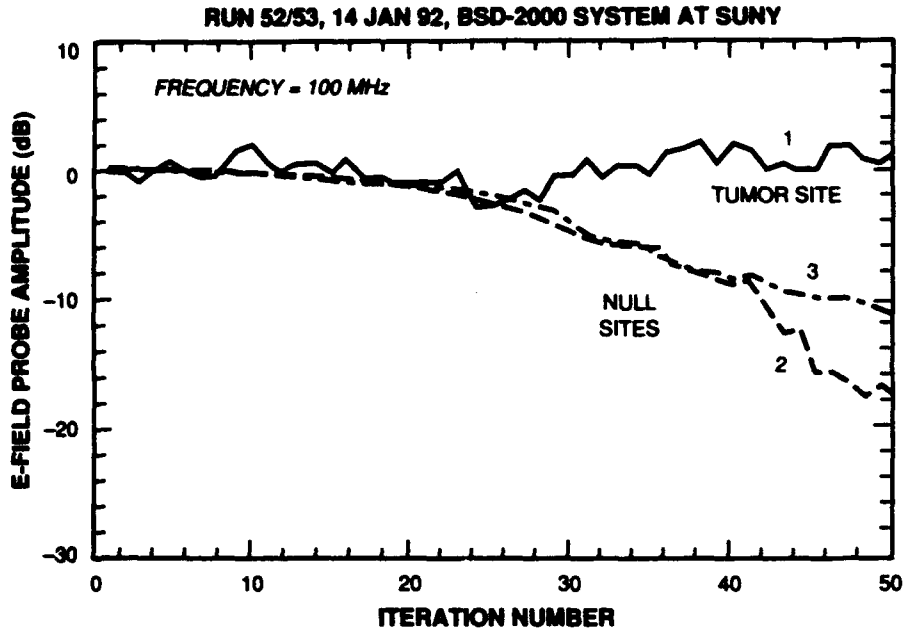
<sup>3</sup>The numbering of transmit-array elements 1,2,3,4 correspond to the anterior, posterior, left, right quadrants, respectively, depicted in Figure 16. Note that "right side" refers the side of the Sigma-60 that contains the coaxial feed cables.

<sup>4</sup>The D/A states are converted to power by a lookup table constructed from calibrated power-meter measurements performed at SUNY.



POSITION	COMMENT	PROBE
1	TUMOR SITE	EP-500
2	NULL SITE	EP-100
3	REF. SITE	EP-400

*Figure 16. Experimental demonstration of an adaptive-nulling hyperthermia system at SUNY. The figure shows the measured electric field as a function of adaptive-nulling gradient-search iteration number for a saline-filled cylindrical phantom. One adaptive null is formed at probe position 2.*



POSITION	COMMENT	PROBE
1	TUMOR SITE	EP-500
2	NULL SITE	EP-100
3	NULL SITE	EP-100

Figure 17. Measured electric field as a function of adaptive-nulling gradient-search iteration number for a saline-filled cylindrical phantom. Two adaptive nulls are formed at probe positions 2 and 3. Notice that the power measured by the invasive electric-field probe is relatively constant over the 50 iterations.

Using the adaptive weights from iteration 50, a measurement of the electric field in the vicinity of one of the nulls was performed. Probe 3 was moved uniformly to nine positions longitudinally on the surface of the cylindrical phantom; the nine positions scanned 20 cm. The electric field before and after nulling is presented in Figure 18. Before nulling, the radiation pattern has broad coverage and the half-power beamwidth is at least 20 cm or more. After nulling, the electric field is reduced at each measurement position over the 20-cm distance. The electric field tends to increase as the probe moves away from the null position at  $y = 0$ . This measured result is consistent with computer simulations where a finite-width null is observed [52].

### 4.3 Adaptive Focus for Cylindrical Phantom

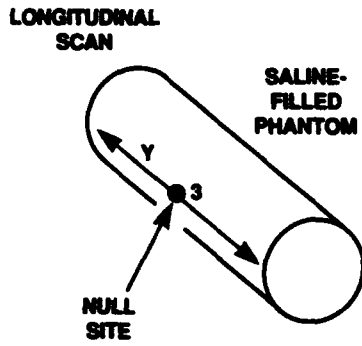
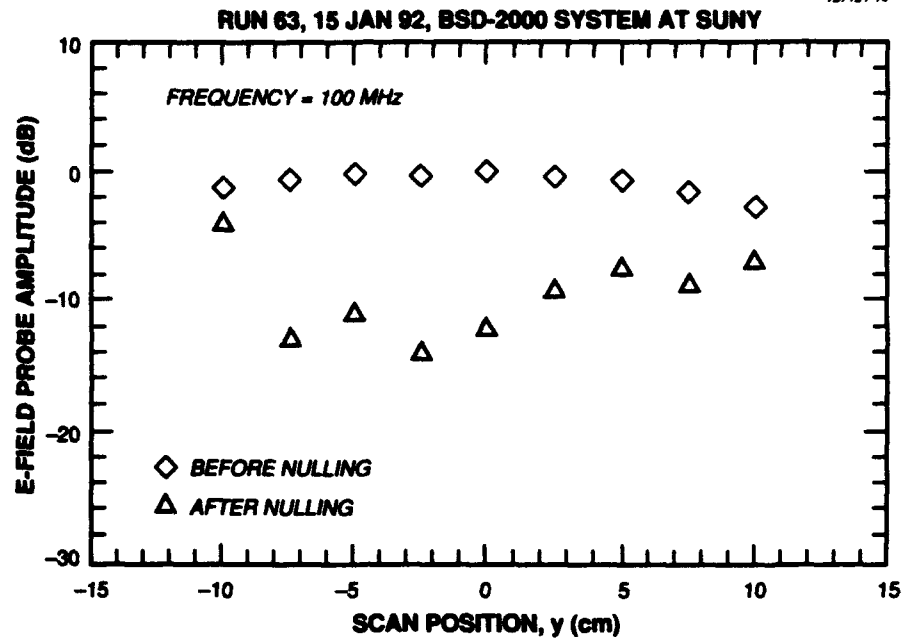
The third experiment involves forming an adaptive focus on the surface of the cylindrical phantom. One EP-100 probe was taped to the right side of the phantom and measured the adaptive-focusing feedback signal. <sup>5</sup> A 30-iteration adaptive-focusing gradient search was executed for this test configuration at 100 MHz. The gradient-search step sizes in terms of raw D/A converter states are  $\Delta A = 0$  and  $\Delta \Phi = 50$ . Because the amplitude step size is zero, only phase focusing is in effect. The initial transmit-weight amplitude states on channels 1 to 4 are (commanded D/A states: 500, 500, 500, 500) or (forward power in watts: 215 W, 215 W, 215 W, 215 W) and the corresponding phase states are (commanded D/A states: 700, 700, 700, 700) or (equivalent phase lag: 100°, 100°, 100°, 100°). After 30 iterations of the focusing algorithm, the transmit-amplitude states are (commanded D/A states: 500, 500, 500, 500) and the corresponding phase states are (commanded D/A states: 1024, 659, 374, 132) or (equivalent phase lag: 113°, 98°, 78°, 30°). The measured electric field as a function of iteration number is displayed in Figure 19. The focal-probe power increases by 0.8 dB over the 30 iterations. The data indicate convergence in about 15 iterations.

### 4.4 One Adaptive Null for Beef Phantom

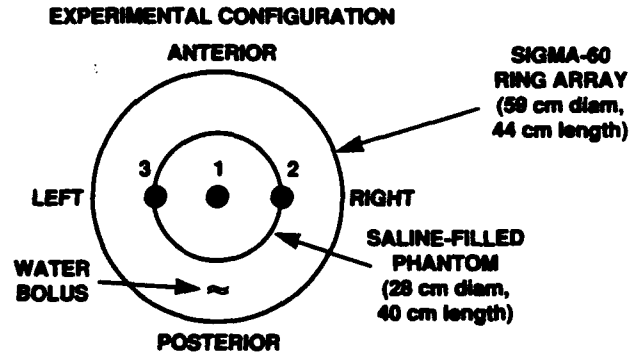
The invasive EP-500 probe is mounted in the center of the beef phantom and measures the electric-field power at the simulated tumor site. An EP-400 probe is taped to the left side of the phantom and an EP-100 probe is taped to the right side of the phantom. Note: The probe positions were already shown in Figure 13. The EP-400 probe measures a reference electric field, while the EP-100 measures the adaptive-nulling feedback signal. A 50-iteration adaptive-nulling gradient search was executed for this test configuration at 120 MHz. The gradient-search step sizes in terms of raw D/A converter states are  $\Delta A = 10$  and  $\Delta \Phi = 50$ . The initial transmit-weight amplitude states on channels 1 to 4 are (commanded D/A states: 500, 500, 500, 500) and the corresponding phase states are (commanded D/A states: 500, 500, 500, 500) or (equivalent phase lag: 103°, 103°, 103°).

---

<sup>5</sup>Note: an attempt was made to focus the array with the EP-500 invasive probe at the center of the phantom. However, the signal level is low (or the array was perfectly focused) so no improvement in focusing was measured.



NOTE: TRANSMIT WEIGHTS ARE FROM RUN 52/53 INTERATION 50



POSITION	COMMENT	PROBE
1	TUMOR SITE	EP-500
2	NULL SITE	EP-100
3	NULL SITE/ SCAN	EP-100

Figure 18. Measured electric field in a longitudinal cut on the surface of the cylindrical phantom before and after nulling.

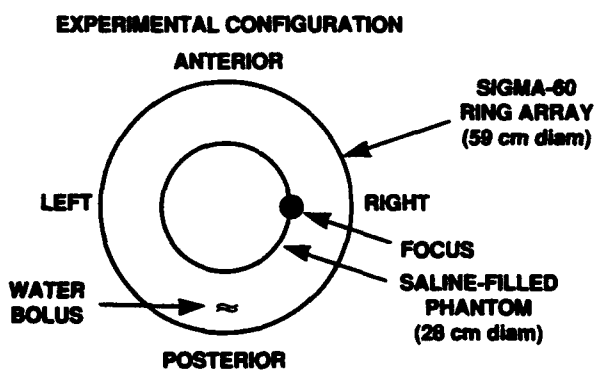
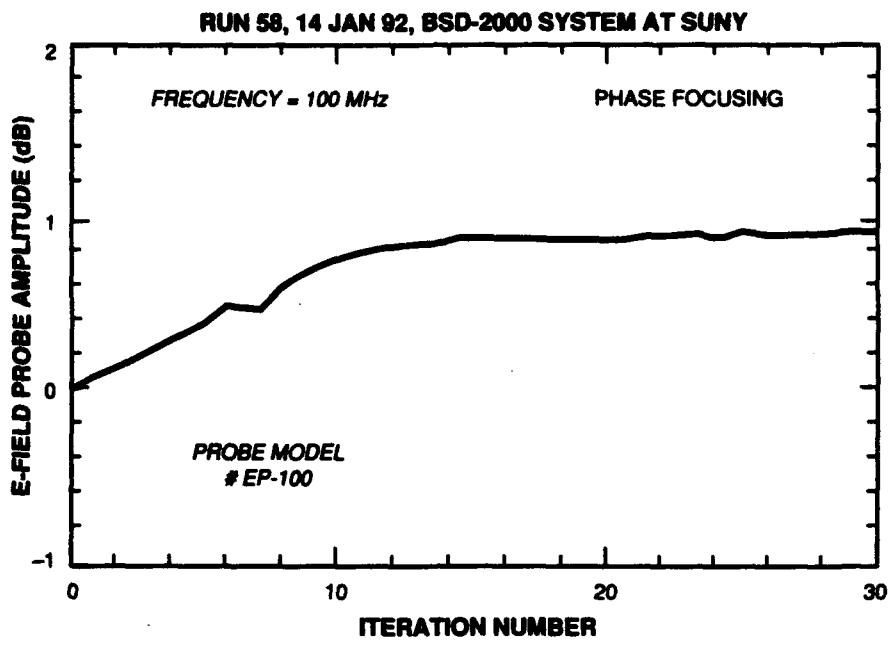


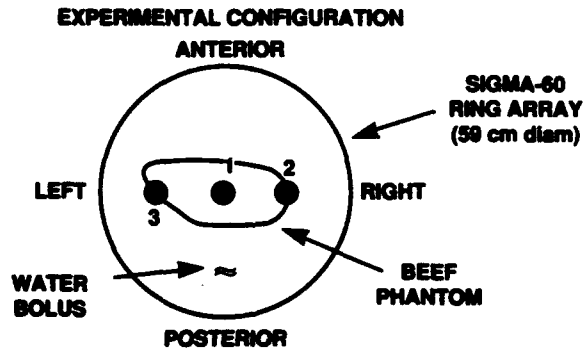
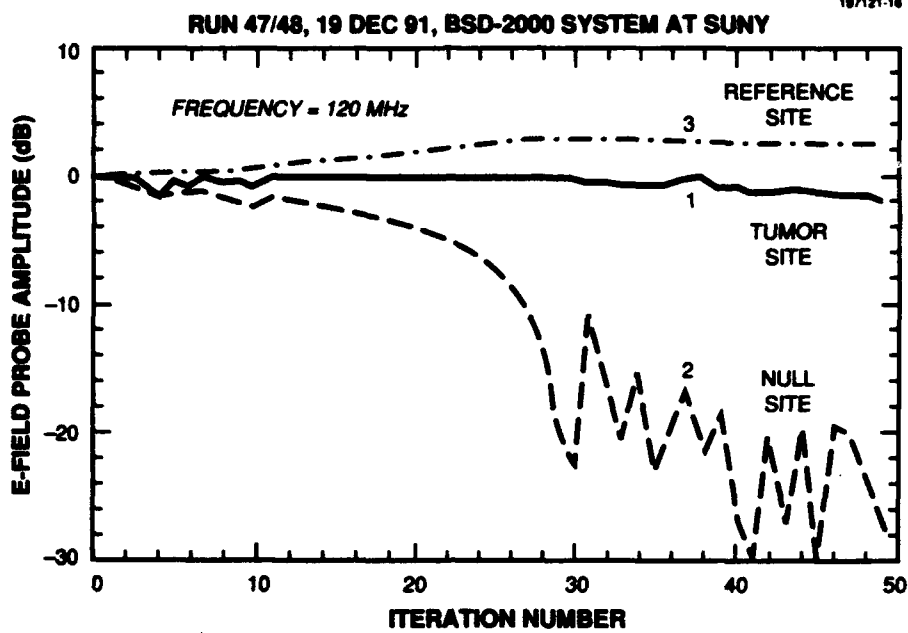
Figure 19. Measured electric field as a function of adaptive-phase-focusing gradient-search iteration number for a saline-filled cylindrical phantom. The power level at the focus increases by 0.8 dB due to the adaptive gradient search.

103°). After 50 iterations of the nulling algorithm, the transmit-amplitude states are (commanded D/A states: 465, 636, 472, 427) or (forward power in watts: 163 W, 390 W, 170 W, 112 W) and the phase states are (commanded D/A states: 278, 195, 188, 988) or (equivalent phase lag: 76°, 60°, 58°, 131°). The measured electric field as a function of iteration number is displayed in Figure 20. The null-site probe power decreases during the first thirty iterations. After 30 iterations, the average null-site amplitude (cancellation) is about -20 dB. The tumor-site power has dropped by about 2 dB at iteration 50; this power reduction is attributed in part to the beam peak shifting away from the focus as observed for the cylindrical phantom. The reference site power is observed to increase by about 2 dB during the 50 iterations.

To record calibrated thermocouple data, the RF was turned off after each 10 iterations<sup>6</sup> for about five minutes. During the period when the RF is off, the temperature-monitoring mode of the BSD-2000 system is accessed and the data recorded. The RF is then turned back on with the transmit weights set to the previous iteration. The measured temperatures at the tumor site and null site are shown in Figure 21. The initial temperatures were approximately equal; after 80 minutes there is a 4°C higher temperature at the tumor site compared to the null site. Thus, the data suggest that adaptive nulling may be effective in improving the thermal distribution in hyperthermia. More detailed thermal measurements in three dimensions have yet to be attempted in this study.

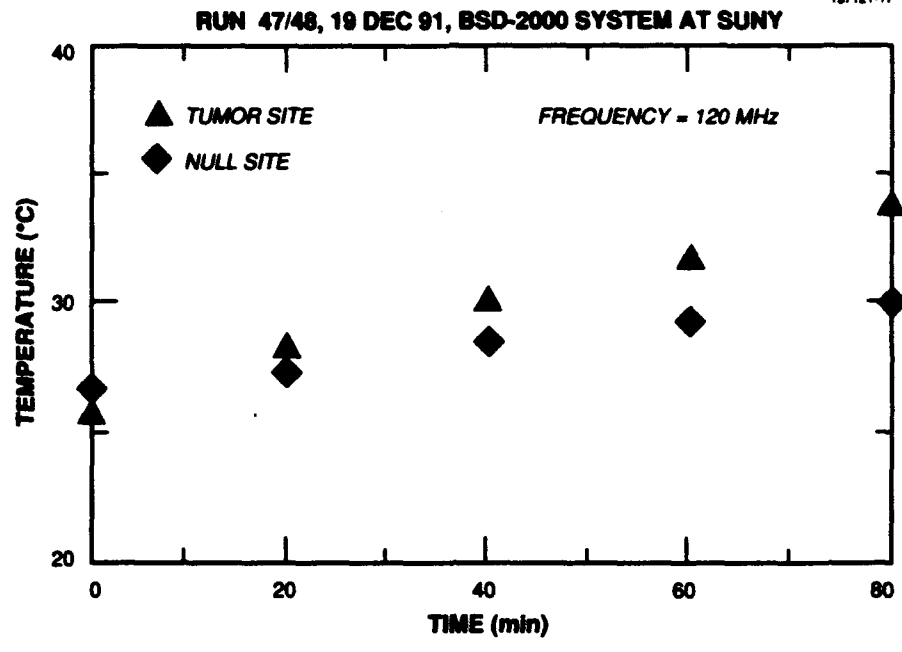
---

<sup>6</sup>The length of time for 10 iterations is approximately 15 minutes with the present software/hardware configuration. A faster iteration speed is required for practical use of the gradient search in patient therapy. By optimizing the software/hardware configuration for adaptive feedback operation, a faster speed should be possible.



POSITION	COMMENT	PROBE
1	TUMOR SITE	EP-500
2	NULL SITE	EP-100
3	REF. SITE	EP-400

Figure 20. Measured electric field as a function of adaptive-nulling gradient-search iteration number for a beef phantom. One adaptive null is formed at probe position 2.



NOTE: RF TURNED OFF FOR ~ 5 min INTERVALS  
DURING TEMPERATURE MEASUREMENTS

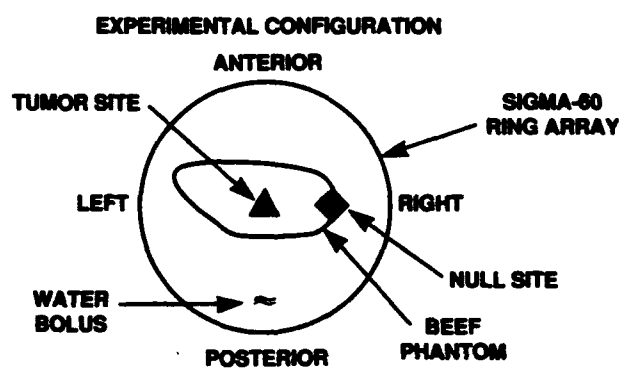


*Figure 21. Measured temperatures in the beef phantom. Eighty minutes after the start of the experiment, a 4° C higher temperature exists at the tumor site compared to the null site.*

## 5. CONCLUSION

An adaptive hyperthermia system has been experimentally demonstrated by modifying a commercial hyperthermia system at the State University of New York Health Science Center at Syracuse. The measurements shown in this report demonstrate that the electric-field radiation pattern of a hyperthermia phased array can be controlled by an adaptive algorithm. Both electric-field nulling (power minimization) and electric-field focusing (power maximization) at desired phantom target positions are experimentally demonstrated. The body of this work consists of electric field measurements; however, limited beef-phantom temperature data were also measured and shown.

The purpose of electric-field nulling is to reduce the occurrence of undesired hot spots inside or on the surface of the target body. In contrast, electric-field focusing is intended to maximize the RF power delivered to a tumor site. The data presented in this report suggest that both of these goals may be achieved with an adaptive hyperthermia phased-array system.

In this report, the adaptive algorithm is a gradient-search feedback technique (method of steepest descent/ascent) derived in Section 2. The gradient search employs transmit-weight gain and phase dithering together with electric-field probe-power measurements, at the desired target positions, to calculate the required gradient-search directions for RF nulling. For RF focusing, a phase-only transmit-weight dithering algorithm was used.

The hyperthermia system investigated here is the BSD Medical Corporation Model BSD-2000 with Sigma-60 phased-array antenna applicator. The array consists of four transmit channels connected to four pairs of dipole radiators. Short-dipole electric field sensors are used to provide feedback amplitude signals for the adaptive array. Two phantom targets were investigated in this report: a homogeneous saline-filled cylindrical target and a heterogeneous (tissue, bone, and fat) beef target. One and two independent adaptive electric-field nulls have been attempted and demonstrated with the saline-filled cylindrical phantom at 100 MHz. The electric-field longitudinal surface distribution was measured before and after adaptive nulling with the saline-filled cylindrical phantom. The longitudinal field-probe measurements indicate a finite-width null characteristic. An adaptive focus was measured with an electric-field probe positioned on the surface of the cylindrical phantom. One adaptive null was attempted and demonstrated at 120 MHz with the beef phantom. During the adaptive-nulling beef-phantom testing, the measured thermocouple data indicate a 4°C higher tumor-site temperature compared to the temperature at the surface of the beef. The measured adaptive null strengths were on the order of -10 dB to -30 dB. For practical implementation of the adaptive-nulling algorithm the required minimum null strength for local near-surface hot-spot reduction is assumed to be on the order of -3 dB to -6 dB, which is readily achieved.

The measured phantom data are encouraging and indicate that a potential improvement in hyperthermia thermal dose exists with adaptive array control. Further experiments are planned.

## APPENDIX A

### Measured Electric-Field Probe Raw Data

Measured Raw A/D Converter Data for Field Probes

One Bull, Cylindrical Phantom (Run 36)

j = iteration number  
P1= probe 1 (tumor site)  
P2= probe 2 (null site)  
P3= probe 3 (reference site)

j	P1	P2	P3
1	24	644	335
2	23	665	355
3	25	658	348
4	22	637	350
5	23	620	347
6	35	600	347
7	31	585	347
8	31	570	350
9	31	551	347
10	31	539	346
11	26	519	351
12	27	500	343
13	27	483	340
14	25	464	340
15	24	448	341
16	29	445	334
17	29	423	332
18	27	409	333
19	18	389	332
20	20	371	330
21	19	350	330
22	19	336	330
23	16	303	338
24	19	295	329
25	21	285	330
26	21	271	329
27	20	260	330
28	23	234	330
29	22	222	330
30	24	206	326
31	24	197	325
32	23	187	324
33	18	159	326
34	19	159	321
35	19	151	318
36	19	132	317
37	17	111	317
38	18	96	311
39	16	71	308
40	14	38	307
41	15	69	317
42	16	61	309
43	12	29	300
44	10	2	301

45 9 6 301  
46 9 2 302  
47 12 21 305  
48 10 4 304  
49 12 15 304  
50 9 2 306

Two Falls, Cylindrical Phantom (Run 52/53)

j = iteration number  
P1= probe 1 (tumor site)  
P2= probe 2 (null site)  
P3= probe 3 (null site)

j	P1	P2	P3
1	19	421	479
2	19	435	497
3	16	430	487
4	20	428	482
5	23	423	491
6	19	414	488
7	17	412	484
8	18	410	485
9	27	401	475
10	30	394	467
11	21	388	462
12	18	379	447
13	21	372	439
14	21	363	431
15	18	357	425
16	23	348	413
17	16	337	405
18	16	329	395
19	15	318	385
20	15	307	374
21	15	291	356
22	15	281	349
23	18	266	332
24	10	251	317
25	10	233	300
26	11	213	280
27	13	197	259
28	11	180	236
29	17	156	208
30	17	138	180
31	22	126	137
32	16	122	126
33	20	111	121
34	20	106	119
35	17	104	103
36	25	80	91
37	26	71	82
38	29	65	77
39	20	57	74
40	29	52	65
41	26	57	72
42	18	36	63
43	20	22	54
44	18	24	52
45	18	11	47
46	28	11	46
47	28	9	45
48	22	7	42
49	20	9	37
50	23	6	33

Focus on Surface of Cylindrical Phantom (Run 58)

j = iteration number  
P1 = probe 1 (tumor site)

j	P1
1	524
2	531
3	541
4	551
5	560
6	573
7	572
8	590
9	601
10	609
11	615
12	620
13	621
14	623
15	627
16	627
17	629
18	627
19	629
20	628
21	630
22	631
23	634
24	631
25	633
26	631
27	632
28	631
29	633
30	631

One Hull, Beef Phantom (Run 47/48)

j = iteration number  
P1= probe 1 (tumor site)  
P2= probe 2 (null site)  
p3= probe 3 (reference site)

j	P1	P2	P3
1	55	905	238
2	55	856	242
3	55	785	247
4	39	670	250
5	51	740	251
6	49	706	257
7	56	743	256
8	50	670	259
9	53	656	263
10	48	566	269
11	56	673	275
12	57	642	281
13	58	600	292
14	58	567	300
15	58	536	307
16	58	500	315
17	58	468	323
18	58	435	333
19	58	402	341
20	58	373	351
21	57	348	356
22	57	304	367
23	57	264	379
24	57	223	390
25	57	178	404
26	56	134	417
27	55	90	429
28	55	47	443
29	54	9	448
30	53	5	451
31	49	79	465
32	52	19	456
33	49	8	445
34	48	25	449
35	49	5	440
36	48	11	437
37	53	21	431
38	54	6	439
39	46	14	429
40	45	2	426
41	40	1	416
42	42	9	414
43	43	2	412
44	43	10	412
45	42	1	409
46	41	10	412
47	39	9	414
48	39	4	412
49	37	2	406

## REFERENCES

1. M.I. Skolnik, *Introduction to Radar Systems*, Second Edition, McGraw-Hill Book Company, 1980.
2. R.T. Compton, Jr., *Adaptive Antennas, Concepts and Performance*, Prentice Hall, New Jersey, 1988.
3. A.J. Fenn, "Application of adaptive nulling to electromagnetic hyperthermia for improved thermal dose distribution in cancer therapy," Technical Report 917, Lincoln Laboratory, Massachusetts Institute of Technology, 3 July 1991. DTIC AD-A241026.
4. A.J. Fenn, "Focused near-field nulling for adaptive electromagnetic hyperthermia applications," *1991 Progress in Electromagnetics Research Symposium Proceedings*, 1-5 July 1991, p. 393.
5. A.J. Fenn, "Adaptive hyperthermia for improved thermal dose distribution," in *Radiation Research: A Twentieth-Century Perspective, Volume I: Congress Abstracts, 7-12 July 1991*, J.D. Chapman, W.C. Dewey, and G.F. Whitmore, Editors, Academic Press, Inc., San Diego, California, 1991, p. 290.
6. A.J. Fenn, "Noninvasive adaptive nulling for improved hyperthermia thermal dose distribution," *IEEE Engineering in Medicine and Biology Society International Conference*, October 31-November 3, 1991, Vol. 13, No. 2, pp. 976-977.
7. G.A. King and A.J. Fenn, "Adaptive nulling measurements with the BSD Sigma-60 applicator for improved hyperthermia thermal distribution," submitted to the Sixth International Congress on Hyperthermic Oncology, April 26-May 1, 1992.
8. C.A. Perez and L.W. Brady, *Principles and Practice of Radiation Oncology*, J.B. Lippincott Co., Philadelphia, 1987.
9. A.W. Guy, "History of biological effects and medical applications of microwave energy," *IEEE Transactions on Microwave Theory and Techniques*, Vol. MTT-32, No. 9, pp. 1182-1200, September 1984.
10. J. Overgaard, "The effect of local hyperthermia alone and in combination with radiation on solid tumors," in *Cancer Therapy by Hyperthermia and Radiation, Proceedings of the 2<sup>nd</sup> International Symposium*, C. Streffer (Editor), 2-4 June 1977, pp. 49-61, Urban & Schwarzenberg, Inc., Baltimore, 1978.
11. J. Overgaard, "Clinical hyperthermia, an update," *Proceedings of the 8th International Congress of Radiation Research*, Vol. 2, pp. 942-947, July 1987.
12. S.B. Field and J.W. Hand, editors, *An Introduction to the Practical Aspects of Clinical Hyperthermia*, Taylor & Francis, London, 1990.

## REFERENCES

(Continued)

13. "Special issue on phased arrays for hyperthermia treatment of cancer," *IEEE Transactions on Microwave Theory and Techniques*, Vol. MTT-34, No. 5, May 1986.
14. "Special issue on hyperthermia and cancer therapy," *IEEE Transactions on Biomedical Engineering*, Vol. BME-31, No. 1, January 1984.
15. V. Sathiaselvan, M.F. Iskander, G.C.W. Howard, and N.M. Bleehen, "Theoretical analysis and clinical demonstration of the effect of power control using the annular phased-array hyperthermia system," *IEEE Transactions on Microwave Theory and Techniques*, Vol. MTT-34, No. 5, pp. 514-519, May 1986.
16. V. Sathiaselvan, "Potential for patient-specific optimization of deep heating patterns through manipulation of amplitude and phase," *Strahlentherapie Onkologie*, Vol. 165, No. 10, pp. 743-745, 1989.
17. D. Sullivan, "Three-dimensional computer simulation in deep regional hyperthermia using the finite-difference time-domain method," *IEEE Transactions on Microwave Theory and Techniques*, Vol. MTT-38, No. 2, pp. 204-211, February 1990.
18. B.S. Trembly, A.H. Wilson, M.J. Sullivan, A.D. Stein, T.Z. Wong, and J.W. Strohbehn, "Control of the SAR pattern within an interstitial microwave array through variation of antenna driving phase," *IEEE Transactions on Microwave Theory and Techniques*, Vol. MTT-34, No. 5, pp. 568-571, May 1986.
19. G. Sato, C. Shibata, S. Sekimukai, H. Wakabayashi, K. Mitsuka, and K. Giga, "Phase-controlled circular array heating equipment for deep-seated tumors: preliminary experiments," *IEEE Transactions on Microwave Theory and Techniques*, Vol. MTT-34, No. 5, pp. 520-525, May 1986.
20. P.A. Cudd, A.P. Anderson, M.S. Hawley, and J. Conway, "Phased-array design considerations for deep hyperthermia through layered tissue," *IEEE Transactions on Microwave Theory and Techniques*, Vol. MTT-34, No. 5, pp. 526-531, May 1986.
21. N. Morita, T. Hamasaki, and N. Kumagai, "An optimal excitation method in multiapplicator systems for forming a hot zone inside the human body," *IEEE Transactions on Microwave Theory and Techniques*, Vol. MTT-34, No. 5, pp. 532-538, May 1986.
22. C. De Wagter, "Optimization of simulated two-dimensional temperature distributions induced by multiple electromagnetic applicators," *IEEE Transactions on Microwave Theory and Techniques*, Vol. MTT-34, No. 5, pp. 589-596, May 1986.
23. M. Knudsen and U. Hartmann, "Optimal temperature control with phased-array hyperthermia system," *IEEE Transactions on Microwave Theory and Techniques*, Vol. MTT-34, No. 5, pp. 597-603, May 1986.

## REFERENCES

(Continued)

24. C.F. Babbs, V.A. Vaguine, and J.T. Jones, "A predictive-adaptive, multipoint feedback controller for local heat therapy of solid tumors," *IEEE Transactions on Microwave Theory and Techniques*, Vol. MTT-34, No. 5, pp. 604-611, May 1986.
25. R.B. Roemer, "Physical and engineering aspects of hyperthermia," *Proceedings of the 8th International Congress of Radiation Research*, Vol. 2, pp. 948-953, July 1987.
26. R.B. Roemer, K. Hynynen, C. Johnson, and R. Kress, "Feedback control and optimization of hyperthermia heating patterns: present status and future needs," *IEEE Eighth Annual Conference of the Engineering in Medicine and Biology Society*, pp. 1496-1499, November 1986.
27. R.B. Roemer, "Optimal power deposition in hyperthermia. I. The treatment goal: the ideal temperature distribution: the role of large blood vessels," *International Journal of Hyperthermia*, Vol. 7, No. 2, pp. 317-341, March-April 1991.
28. A. Boag and Y. Leviatan, "Optimal excitation of multiapplicator systems for deep regional hyperthermia," *IEEE Transactions on Biomedical Engineering*, Vol. BME-37, No. 10, pp. 987-995, October 1990.
29. P. Wust, J. Nadobny, R. Felix, P. Deuffhard, A. Louis, and W. John, "Strategies for optimized application of annular-phased-array systems in clinical hyperthermia," *International Journal of Hyperthermia*, Vol. 7, No. 1, pp. 157-173, January-February 1991.
30. D.B. Nguyen and J.W. Strohbehn, "Optimal positions, orientations, amplitudes and phases of movable microwave applicators in hyperthermia treatment," *Hyperthermic Oncology 1988*, Vol. 1, T. Sugahara and M. Saito (editors), Taylor & Francis, London, pp. 738-739, 1989.
31. J.W. Strohbehn, E.H. Curtis, K.D. Paulsen, and D.R. Lynch, "Optimization of the absorbed power distribution for an annular phased-array hyperthermia system," *International Journal of Radiation Oncology, Biology, Physics*, Vol. 16, pp. 589-599, 1989.
32. J.T. Loane III and S.W. Lee, "Gain optimization of a near-field focusing array for hyperthermia applications," *IEEE Transactions on Microwave Theory and Techniques*, Vol. 37, No. 10, pp. 1629-1635, October 1989.
33. P.F. Turner, T. Schaefermeyer, and T. Saxton, "Future trends in heating technology of deep-seated tumors," *Recent Results in Cancer Research*, Vol. 107, pp. 249-262, 1988.
34. P.F. Turner, A. Tumeh, and T. Schaefermeyer, "BSD-2000 approach for deep local and regional hyperthermia: physics and technology," *Strahlentherapie Onkologie*, Vol. 165, No. 10, pp. 738-741, 1989.

## REFERENCES

(Continued)

35. H.I. Bassen and G.S. Smith, "Electric Field Probes—A Review," *IEEE Transactions on Antennas and Propagation*, Vol. AP-31, No. 5, September 1983.
36. A. Uhler, "Characterization of crystal diodes for low-level microwave detection," *The Microwave Journal*, pp. 59–67, July 1963.
37. M. Astrahan, K. Imanaka, G. Jozsef, F. Ameye, L. Baert, M.D. Sapozink, S. Boyd, and Z. Petrovich, "Heating characteristics of a helical microwave applicator for transurethral hyperthermia of benign prostatic hyperplasia," *International Journal of Hyperthermia*, Vol. 7, No. 1, pp. 141–155, 1991.
38. A.J. Fenn, "Theory and analysis of near-field adaptive nulling," *1986 IEEE Antennas and Propagation Society International Symposium Digest*, Vol. 2, IEEE, New York, pp. 579–582, 1986.
39. A.J. Fenn, "Theory and analysis of near-field adaptive nulling," *1986 Asilomar Conf. on Signals, Systems and Computers*, Computer Society Press of the IEEE, Washington, D.C., pp. 105–109, 1986.
40. A.J. Fenn, "Theoretical near-field clutter and interference cancellation for an adaptive phased-array antenna," *1987 IEEE Antennas and Propagation Society International Symposium Digest*, Vol. 1, IEEE, New York, pp. 46–49, 1987.
41. A.J. Fenn, "Moment-method analysis of near-field adaptive nulling," *IEEE Sixth International Conference on Antennas and Propagation, ICAP 89*, 4–7 April 1989, pp. 295–301.
42. A.J. Fenn, "Evaluation of adaptive phased-array antenna far-field nulling performance in the near-field region," *IEEE Transactions on Antennas and Propagation*, Vol. 38, No. 2, pp. 173–185, February 1990.
43. A.J. Fenn, "Near-field testing of adaptive radar systems," *Proc. 12th Annual Antenna Measurement Techniques Association Meeting and Symposium*, 8–11 October 1990, pp. 13–9–13–14.
44. A.J. Fenn, H.M. Aumann, F.G. Willwerth, and J.R. Johnson, "Focused near-field adaptive nulling: experimental investigation," *1990 IEEE Antennas and Propagation Society International Symposium Digest*, Vol. 1, 7–11 May 1990, pp. 186–189.
45. J.R. Johnson, A.J. Fenn, H.M. Aumann, and F.G. Willwerth, "An experimental adaptive nulling receiver utilizing the sample matrix inversion algorithm with channel equalization," *IEEE Transactions on Microwave Theory and Techniques*, Vol. 39, No. 5, pp. 798–808, May 1991.
46. D.J. Farina and R.P. Flam, "A self-normalizing gradient-search adaptive array algorithm," *IEEE Transactions on Aerospace and Electronic Systems*, Vol. 27, No. 6, pp. 901–905, November 1991.

**REFERENCES**  
(Continued)

47. A. Cantoni, "Application of orthogonal perturbation sequences to adaptive beamforming," *IEEE Trans. Antennas Propagat.*, Vol. Ap-28, No. 2, pp. 191-202, March 1980.
48. L.C. Godara and A. Cantoni, "Analysis of the performance of adaptive beamforming using perturbation sequences," *IEEE Trans. Antennas Propagat.*, Vol. AP-31, No. 2, pp. 268-279, March 1983.
49. D.C. Farden and R.M. Davis, "Orthogonal weight perturbation algorithms in partially adaptive arrays," *IEEE Trans. Antennas Propagat.* Vol. AP-33, No. 1, pp. 56-63, January 1985.
50. R.L. Zahradnik, *Theory and Techniques of Optimization for Practicing Engineers*, Barnes and Noble, New York, pp. 118-124, 1971.
51. A.J. Fenn, "Maximizing jammer effectiveness for evaluating the performance of adaptive nulling array antennas," *IEEE Trans. Antennas Propagat.*, Vol. AP-33, No. 10, pp. 1131-1142, October 1985.
52. A.J. Fenn, "Application of adaptive nulling for improving the thermal distribution in electromagnetic hyperthermia," submitted to the Applied Computational Electromagnetics Society Special Issue on Bioelectromagnetic Computations.

# REPORT DOCUMENTATION PAGE

**Form Approved**  
**OMB No. 0704-0188**

Public reporting burden for this collection of information is estimated to average 1 hour per response, including the time for reviewing instructions, searching existing data sources, gathering and maintaining the data needed, and completing and reviewing the collection of information. Send comments regarding this burden estimate or any other aspect of this collection of information, including suggestions for reducing this burden, to Washington Headquarters Service, Directorate for Information Operations and Reports, 1215 Jefferson Davis Highway, Suite 1204, Arlington, VA 22202-4302, and to the Office of Management and Budget, Paperwork Reduction Project (0704-0188), Washington, DC 20503.

<b>1. AGENCY USE ONLY (Leave blank)</b>	<b>2. REPORT DATE</b> 19 November 1993	<b>3. REPORT TYPE AND DATES COVERED</b> Technical Report	
<b>4. TITLE AND SUBTITLE</b>  An Adaptive Radio-Frequency Hyperthermia Phased-Array System for Improved Cancer Therapy: Phantom Target Measurements		<b>5. FUNDING NUMBERS</b>  C — F19628-90-C-0002 PE — 33110F, 33603F, 63226E PR — 370	
<b>6. AUTHOR(S)</b>  Alan J. Fenn and Gerald A. King		<b>8. PERFORMING ORGANIZATION REPORT NUMBER</b>  TR-999	
<b>7. PERFORMING ORGANIZATION NAME(S) AND ADDRESS(ES)</b>  Lincoln Laboratory, MIT P.O. Box 73 Lexington, MA 02173-9108		<b>10. SPONSORING/MONITORING AGENCY REPORT NUMBER</b>  ESC-TR-93-299	
<b>9. SPONSORING/MONITORING AGENCY NAME(S) AND ADDRESS(ES)</b>  HQ Electronic Systems Center/ENK (AFMC) Hanscom AFB Bedford, MA 01731-5000		<b>11. SUPPLEMENTARY NOTES</b>	
<b>12a. DISTRIBUTION/AVAILABILITY STATEMENT</b>  Approved for public release; distribution is unlimited.		<b>12b. DISTRIBUTION CODE</b>	
<b>13. ABSTRACT (Maximum 200 words)</b>  An adaptive radio-frequency hyperthermia system for improved therapeutic tumor heating is investigated. Adaptive array techniques are used to modify the electric-field and temperature distribution in hyperthermia experiments with phantom targets. A commercial hyperthermia phased-array antenna system at the SUNY Health Science Center in Syracuse, New York, has been modified to implement adaptive nulling and adaptive focusing algorithms. The hyperthermia system is the BSD Medical Corporation Model BSD-2000 with Sigma-60 annular phased-array antenna applicator. The applicator operates from 60 to 120 MHz and consists of four pairs of dipole antenna radiators. The four-channel transmit array is made adaptive by software modifications which invoke a gradient-search feedback algorithm. The gradient-search algorithm implements the method of steepest descent for adaptive nulling and the method of steepest ascent for adaptive focusing. The feedback signals are provided by electric-field short-dipole probe antennas.  With the proposed adaptive hyperthermia array design concept, it may be possible to maximize the applied electric field at a tumor position in the target body and simultaneously minimize or reduce the electric field at target positions where undesired high-temperature regions (hot spots) occur. The measured phantom-target data indicate that adaptive nulling can reduce the electric field at one or more target positions while simultaneously focusing at a deep-seated position within the target.			
<b>14. SUBJECT TERMS</b> tumor heating                      adaptive phased array microwave hyperthermia        adaptive focusing cancer therapy		<b>15. NUMBER OF PAGES</b> 66	
<b>17. SECURITY CLASSIFICATION OF REPORT</b> Unclassified		<b>16. PRICE CODE</b>	
<b>18. SECURITY CLASSIFICATION OF THIS PAGE</b> Unclassified	<b>19. SECURITY CLASSIFICATION OF ABSTRACT</b> Unclassified	<b>20. LIMITATION OF ABSTRACT</b> Same As Report	